University *of Ljubljana*
Faculty *of Mathematics and Physics*

**PILOT PROJECT ON CLIMATE CHANGE:
BUILDING THE LINK BETWEEN FLOOD RISK MANAGEMENT PLANING AND CLIMATE CHANGE ASSESSEMENT IN THE SAVA RIVER BASIN**

COMPONENT A3: COMPILATION OF VARIOUS EXISTING CLIMATE CHANGE SCENARIOS FOR THE REGION, THEIR EXPECTED IMPACTS ON WATER CYCLE AND MORE SPECIFICALLY ON FREQUENCY AND MAGNITUDE OF EXTREME FLOOD EVENTS

Part 1: REPORT ON METEOROLOGICAL PART OF DEVELOPMENT OF CLIMATE PROJECTIONS FOR THE SAVA RIVER BASIN

November 2013

This report has been produced in the framework of the project "Testing of the Guidance document developed under the Water Convention (UNECE) - Building the link between the flood risk management planning and climate change assessment in the Sava River Basin", implemented in the framework of the Environment and Security Initiative (ENVSEC) by the International Sava Commission (ISRBC) and the United Nations Economic Commission for Europe (UNECE) with funding from Finland. The countries sharing the Sava River Basin, together with the ISRBC (www.savacommision.org), appreciate this successful cooperation and kind support.

Participated in the study:

The Faculty of Mathematics and Physics, Chair of Meteorology

Prof. Jože RAKOVEC, PhD and
Andrej CEGLAR. PhD

DISCLAIMER

TABLE OF CONTENTS:

1 INTRODUCTION

Outputs from Global Climate Models (GCMs) cannot be used to force hydrological or other impact models without some form of prior bias correction if realistic output is sought (Sharma et al., 2007; Ines and Hansen, 2006). The spatial resolution of GCM simulations is usually too low to simulate the local climate characteristics realistically, since these depend on local terrain features. Outputs from GCMs are therefore downscaled, where a dynamical or statistical approach can be used (Mearns et al., 1999). Dynamic and statistical downscaling techniques are often presented as mutually exclusive but they can often be used together (Segui et al., 2009). Downscaled simulations are then used as input for impact models. Statistical downscaling relies on the stationarity assumption regarding the relationship between local or regional climate variability and simulated climate variability on large scale. This, however, is not a trivial assumption (Trenberth et al., 2003).

A complete and thorough impact study should take into consideration different sources of uncertainty, which can be computationally quite expensive. There are three major sources of uncertainty, which enter into impact assessment at different stages of impact modeling. These are related to emission scenario, climate model structure and parameterization schemes (Reaney and Fowler, 2008). Simulations of Regional Climate Models (RCMs) are influenced by spatial and temporal resolution, numerical scheme, physical parameterizations and boundary conditions (Deque et al., 2007). Impact assessment models add a new source of uncertainty, which originates from the physical processes in the impact models.

The uncertainty cascade in impact studies can be addressed with an ensemble approach. The ensemble approach addresses the impact of climate change, whereby the uncertainties from CO_2 emission scenario, climate change scenarios and physical processes in impact assessment models can be taken into account (Tao et al., 2009). It is, however, very unlikely that any experiment ensemble can represent the full range of uncertainties related to the future greenhouse gas emissions and the choice of GCM and RCM. Furthermore, RCM simulations can be subject to considerable biases when comparing the simulated control climate to observations. Biases in climate model simulations originate from the numerical solutions of the differential equations, parameterizations of sub-grid scale processes and limited resolution. Use of these simulations to force the impact models can result in unrealistic outputs (Sharma et al., 2007). Even though it is customary for climate modelers to present future global or regional temperature or precipitation changes in terms of relative changes, we still need a realistic representation of climate variables to force the impact models (Semenov and Doblas-Reyes, 2007; Schneider et al., 2007).

Multi-model ensemble combination has become a standard technique to improve ensemble forecasts on all time scales, including climate time scales (decades or centuries). The multi-model ensemble can locally outperform a best-model approach, but only if the single-model ensembles are overconfident (Weigel et al., 2008). The reason is that the multi-model combination reduces overconfidence (i.e. ensemble spread is widened), while the average ensemble mean error is reduced. No single model is best at representing all climate processes and variables. Moreover, the quality of model results usually depends on location and time. It is therefore important to apply a weighting methodology, which is relevant to robustness and

uncertainty in model performance. Impact assessment using the RCM output should ideally use at least two or more RCMs forced by two or more GCMs and consider their output in the context of full matrix output to ensure that they do not under-sample uncertainty (van der Linden and Mitchell, 2009).

A realistic representation of precipitation fields in the future climate projections from climate models is crucial for impact and vulnerability assessment (Semenov and Doblas-Reyes, 2007; Schneider et al., 2007; Wood et al., 2004). The resolution of RCMs is often not enough for most hydrological models, thus they need to be further downscaled and bias corrected (Christensen et al., 2008), since most of RCMs are subject to a systematic error in precipitation. The result is that too many days with very low precipitation intensity and too few dry days are generated. Therefore, impact modelers often use bias correction techniques that correct all ranges of the intensity histogram (Ceglar and Kajfež-Bogataj, 2012; Baigorria et al., 2007). This involves derivation of transfer functions from observed and simulated cumulative probability distributions. When applying a hindcast derived correction to simulations of projected climate, we have to assume that the transfer function has the same form (Piani et al., 2010). The transfer function between raw and corrected climate model simulations should therefore be robust, which is the case when it depends on fewer parameters to be derived from the data.

The aim of the proposed study was to 1) assess the quality of daily precipitation and temperature simulations from the ENSEMBLES RCMs over the Sava river basin, 2) determine the importance of bias correction on simulated daily precipitation and temperature, 3) assess the ability of raw and corrected daily precipitation simulations to simulate extreme precipitation events and 4) calculate bias corrected projections of daily and seasonal precipitation and temperature for the 21st Century.

2 DATA

Meteorological data from simulations of 16 different ENSEMBLES GCM-RCM model runs were used for preparation of projections (Table 1). More detailed information about different climate models used in this study can be found on the project web site (http://ensemblesrt3.dmi.dk). All simulations for the 21st Century were done using only the IPCC SRES A1B emission scenario[1] (Nakičenović et al., 2000), since it has been recognized that the choice of the emission scenario is less relevant until the middle of the 21st Century (van der Linden and Mitchell, 2009). The A1B scenario assumes a future world of rapid economic growth, low population growth and rapid introduction of new and more efficient technologies. Major underlying themes are economic and cultural convergence and capacity building, with a substantial reduction in regional differences in per capita income. It is assumed that

[1] *In IPCC SRES four qualitative storylines yield four sets of scenarios called 'families': A1, A2, B1,* and B2. Altogether 40 SRES scenarios have been developed by six modeling teams. All are equally valid with no assigned probabilities of occurrence. The set of scenarios consists of six scenario groups drawn from the four families: one group each in A2, B1, B2, and three groups within the A1 family, characterizing alternative developments of energy technologies: A1FI (fossil fuel intensive), A1B (balanced), and A1T (predominantly non-fossil fuel). Within each group of scenarios, some share 'harmonized' assumptions on global population, gross world product, and final energy …(*while the others in the group)…* explore uncertainties in driving forces beyond those of the harmonized scenarios … (*adapted from Nakičenović et al, 2000*).

under the A1B scenario, people pursue personal wealth rather than environmental quality.

The horizontal resolution of RCM simulations is 0.25 degree. Simulations generally cover a time period between 1961 and 2100, with the exception of three model runs (Table 1), where the period 1961 - 2050 is covered. Simulations of two different meteorological variables were used in our study: daily precipitation and daily mean air temperature.

In addition, E-OBS data (daily precipitation) were used as a reference (observational) dataset for comparison and derivation of transfer functions. These data have been designed to provide the best estimate of grid box averages to enable a direct comparison with RCMs. The E-OBS dataset was defined on the same 0.25 degree grid resolution. The E-OBS dataset covers the period between 1950 and 2011. Only data between 1961 and 2010 were used in this study.

Table 1: ENSEMBLES GCM-RCM simulations on spatial resolution 0.25 degree, which were used in our study. For METO-HC GCM, there are standard, low and high sensitivity runs (differing by the value of entrainment parameter, which controls the mixing between ascending plumes and the surrounding environment in the HADCM3 parameterization of convection; for details, see van der Linden and Mitchell, 2009)

	RCM									
		C4I RCA3	DMI HIRHAM 5	ETHZ CLM	GKSS CLM	KNMI RACMO2	METNO HIRHAM	METO-HC HADRM	MPI REMO	SMHI RCA
GCM	METO-HC LOW							1951-2100		1951-2100
	METO-HC STD			1951-2100			1951-2050	1951-2100		
	METO-HC HIGH	1951-2100						1951-2100		
	MPIMET ECHAM5		1951-2100			1951-2100			1951-2100	1951-2100
	NERSC BCM		1951-2100				1951-2050			1951-2100
	CNRM ARPEGE		1951-2100							
	IPSL				1951-2050					

Table 2: ENSEMBLES GCM-RCM acronyms, used in figures.

	RCM									
		C4I RCA3	DMI HIRHAM 5	ETHZ CLM	GKSS CLM	KNMI RACMO2	METNO HIRHAM	METO-HC HADRM	MPI REMO	SMHI RCA
GCM	METO-HC LOW							METO-HC_HadRM3Q3_HadRM3Q3		SMHIRCA HadCM3Q3
	METO-HC STD			ETHZ_CLM			METNOHIRHAM_HadCM3Q0	METO-HC_HadRM3Q0_HadRM3Q0		
	METO-HC HIGH	C4IRCA3_HadCM3Q16						METO-HC_HadRM3Q16_HadRM3Q16		
	MPIMET ECHAM5		DMI-HIRHAM5_ECHAM5			KNMI-RACMO2			MPI-M-REMO	SMHIRCA ECHAM5
	NERSC BCM		DMI-HIRHAM5_BCM				METNOHIRHAM_BCM			SMHIRCA BCM
	CNRM ARPEGE		DMI-HIRHAM5-ARPEGE							
	IPSL				GKSS-CCLM4					

3 BIAS CORRECTION OF MODEL SIMULATIONS

A statistical bias correction method was used to correct simulated precipitation for systematic errors (Piani et al., 2010). The method is based on adjusting the cumulative probability distribution function of simulated precipitation to the cumulative distribution function of observed precipitation (E-OBS data). The fundamental assumption is that both, observed and simulated daily precipitation probability distributions, are well approximated by the theoretical probability distribution.

Correction for precipitation was done simultaneously for precipitation frequency and intensity (Ines and Hansen, 2006). Mean rainfall in calendar month *m* is the product of mean intensity (mm/wet day) and relative frequency (wet days/month). Correcting bias of the two rainfall components will therefore correct also the monthly and seasonal rainfall. The correction includes truncating RCM rainfall intensity distribution at a point that approximately reproduces the long-term observed relative frequency of rainfall and then mapping the truncated RCM rainfall onto a gamma distribution fitted to the observed intensity distribution in the E-OBS dataset. We applied the two-step procedure for each of the 12 calendar months.

3.1 CORRECTING RAINFALL FREQUENCY

The frequency of daily RCM rainfall was corrected by fitting a threshold value $\tilde{x}_{GCM}$ to truncate the empirical distribution of the raw daily RCM rainfall under the condition that the mean frequency of rainfall above the threshold matches the observed rainfall frequency. The threshold value can therefore be calculated as:

$$\tilde{x}_{GCM} = F_{GCM}^{-1}(F_{OBS}(\tilde{x}))$$

where F() and F^{-1}() denote a cumulative distribution function and its inverse. A minimum rainfall amount for the observed day to be considered as wet, was 0.1 mm.

3.2 CORRECTING PRECIPITATION INTENSITY

All precipitation values below the threshold value $\tilde{x}_{GCM}$ were set to zero. The resulting time series of precipitation data were then used for correcting precipitation intensity. This was done by mapping the RCM intensity distribution ($F_{I,RCM}(x)$) onto the observed intensity distribution ($F_{I,OBS}(x)$), separately for each month. Zhe corrected daily precipitation intensity is therefore:

$$x' = \begin{cases} F_{I,OBS}^{-1}(F_{I,RCM}(x)); x \geq \tilde{x}_{RCM} \\ 0; x < \tilde{x}_{RCM} \end{cases}.$$

The cumulative distribution functions were fitted to two-parameter gamma distribution:

$$pdf(x) = \frac{e^{-x/\vartheta} x^{k-1}}{\Gamma(k)\vartheta^k},$$

where x is the normalized daily precipitation, k is the shape parameter and ϑ the scale parameter of the gamma function. This is a generally accepted practice for observed precipitation where k>1 (Katz, 1999). The bias correction procedure is illustrated on Figure 1.

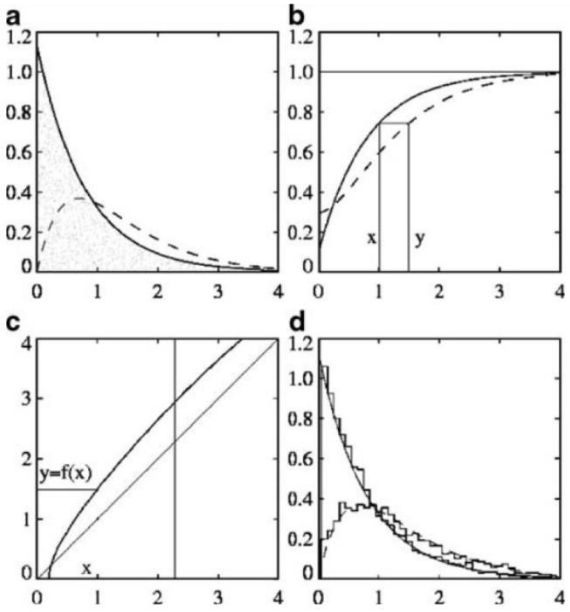

Figure 1: Statistical correction, applied to a synthetic dataset. (a) Synthetic PDF of simulated daily precipitation (solid line), synthetic PDF of observed daily precipitation (dashed line). (b) Cumulative distribution functions obtained by integrating the corresponding PDFs in (a). (c) Transfer function obtained graphically from (b) by solving: $CDF_{obs}(y)=SDF_{sim}(x)$ (thick solid line). (d) Histogram of synthetic dataset given by x-coordinate of points evenly scatter under solid PDF in (a) superimposed onto dashed PDF from (a) (thin dashed line) (Piani et al., 2010).

3.3 CORRECTING TEMPERATURE SIMULATIONS

Bias correction was applied to simulations of daily temperatures as well. The procedure was the same, as described in section 3.2, except the theoretical probability function used to derive the transfer function. In the case of temperature data, the normal probability distribution was used.

3.4 PROCEDURE FOR THE SAVA RIVER BASIN

The bias correction procedure was applied to each of 16 model runs for the Sava river basin. Histograms were defined for each grid point, using the data from 16 model runs and observational data from E-OBS. In the next step, the wet day frequency was corrected, followed by fitting the gamma distribution to simulated and observed precipitation for each grid cell. The parameters of gamma distribution were derived on the basis of the minimization of the square error. 6 parameters were therefore defined for each grid cell: 2 parameters for gamma distribution and 1 parameter for wet day frequency (from simulations and observations). The procedure was repeated for temperature data, using the normal theoretical distribution.

The evaluation of climate models against observed data is an important step in building confidence in their use for impact assessment. The methodology was therefore validated on the control climate data. The transfer function was derived using data from 1961 to 1990. The obtained transfer functions were then applied to RCM simulations from 1991 to 2010. The procedure was repeated for each of climate model runs, each month and each grid cell. To address the issue of mean-based evaluation of climate models, we examined the capacity of climate models to simulate the observed PDFs in the validation period, using daily data from the E-OBS dataset. The skill of each climate model to reproduce the PDF was assessed using a Perkins

skill score (PSS) (Perkins, 2007). PDF based validation has a stronger performance than a mean-based assessment, and therefore provides more confidence in a climate model. However, a model that does well in a PDF could still hide some major limitations (especially extreme events, which are to rare too significantly contribute to the skill score).
The modified match metric for precipitation was therefore constructed to measure the extent that the individual normalized model PDF match the observations for the validation period. PSS is based on the common overlap of the model and observed PDF, where a resulting skill score ranges from 0 to 1 (zero meaning no overlap at all, whereas 1 the perfect model simulations):

$$PSS = \sum_{i=1}^{N} \min(PDF_{sim,i}, PDF_{obs,i}),$$

where $PDF_{sim,i}$ represents the simulated PDF and $PDF_{obs,I}$, the observed PDF for i-th bin. Square root of precipitation was taken for the calculation of PSS and bin width was 0.5 mm. For temperature, bin width 1 C was taken.

For this study, a modified version of the metric was used (Boberg et al., 2007). The precipitation PDF was divided to two parts, which allowed the tail of the distribution with extreme precipitation to influence the final score. For each grid point, 90th percentile of daily precipitation intensity was calculated for each season and was subsequently used to divide the PDF into two parts. The first part was in the range from 0.1 mm/day to 90th percentile, whereas the second part was above 90th percentile. The first part characterized moderate precipitation events, whereas the second part of the PDF characterized extreme precipitation events. Two parts of the PDF are then normalized and PSS is calculated for each of them. The final value of the skill score is calculated as $(PSS_{lower\ tail}+PSS_{upper\ tail})/2$. The modified PSS is better for assessment of the quality of simulation of extreme precipitation events.

3.5 CLIMATE PROJECTIONS FOR THE SAVA RIVER BASIN

Climate projections for the Sava river basin were calculated, based on derived transfer functions for the period 1961–2000. Transfer functions were applied to climate projections for the 21st Century from RCM simulations. Three periods were used for assessing future climate change: 2011–2040, 2041–2070 and 2071–2100. For each of the periods, absolute values for seasonal precipitation and extreme precipitation were determined as well as the differences from the reference period (1971–2000) values. Results are provided in forms of images, where spatial distributions for the Sava river basin for each of the variables are shown.

4 RESULTS WITH DISCUSSION

4.1 VALIDATION OF PRECIPITATION SIMULATIONS

In the first step, the validation of corrected climate model simulations is presented. For each season, mean daily precipitation was calculated as well as mean seasonal precipitation from raw climate model simulations and compared to bias corrected values. The comparison was done for the validation period 1991–2010, where the bias corrected values were calculated based on transfer functions from the period 1961–1990. PSS was used as the model performance measure.

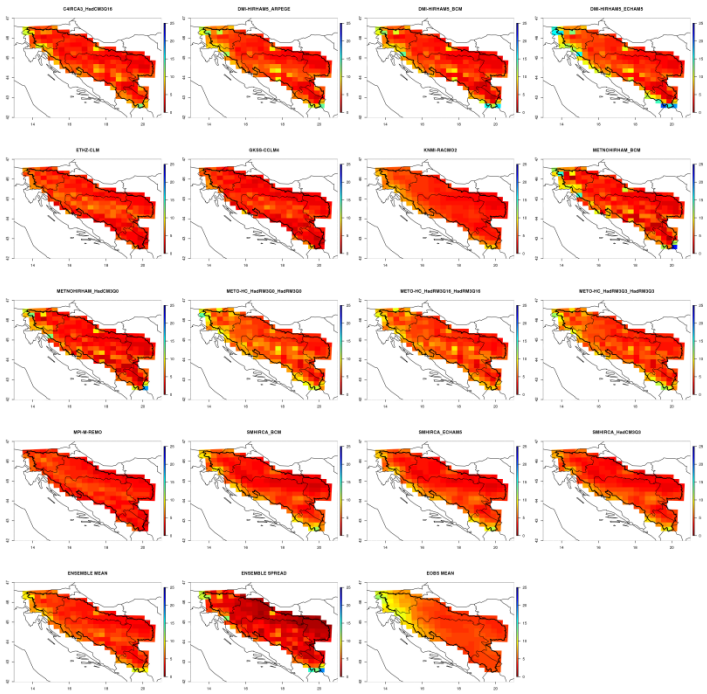

Figure 2: Mean daily precipitation on a wet day in spring for the validation period 1991-2010. Shown are raw simulations with 16 different climate model runs (see table 2 for details), ensemble mean, ensemble spread and observed mean (EOBS MEAN). Unit on all images is mm/day.

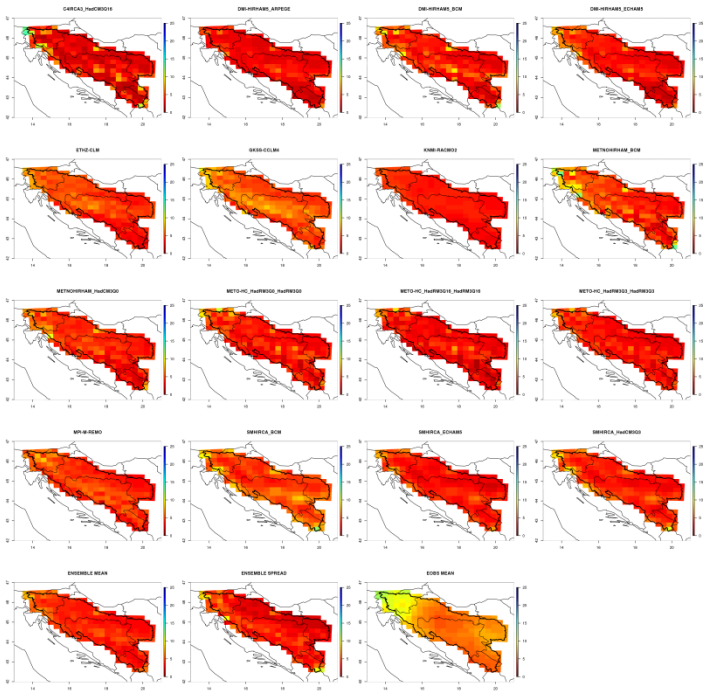

Figure 3: Mean daily precipitation on a wet day in summer for the validation period 1991-2010. Shown are raw simulations with 16 different climate model runs (see table 2 for details), ensemble mean, ensemble spread and observed mean (EOBS MEAN). Unit on all images is mm/day.

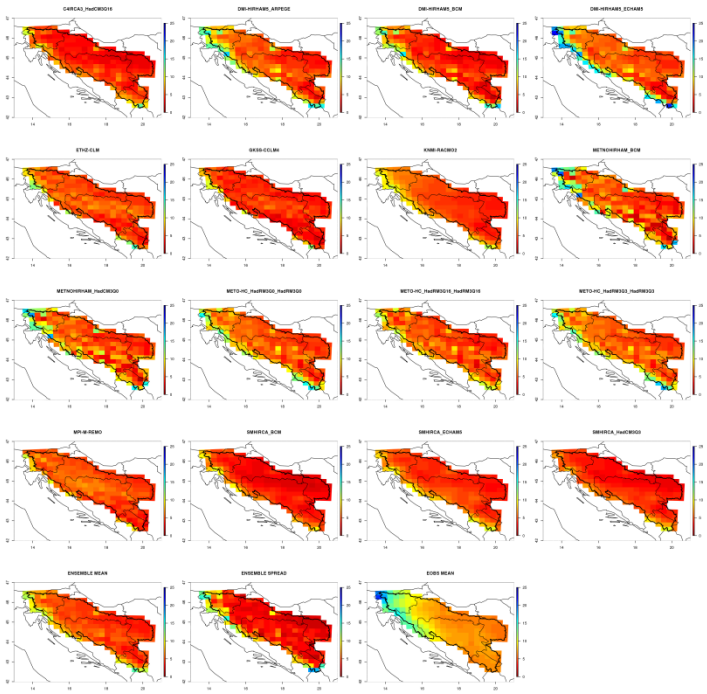

Figure 4: Mean daily precipitation on a wet day in autumn for the validation period 1991-2010. Shown are raw simulations with 16 different climate model runs (see table 2 for details), ensemble mean, ensemble spread and observed mean (EOBS MEAN). Unit on all images is mm/day.

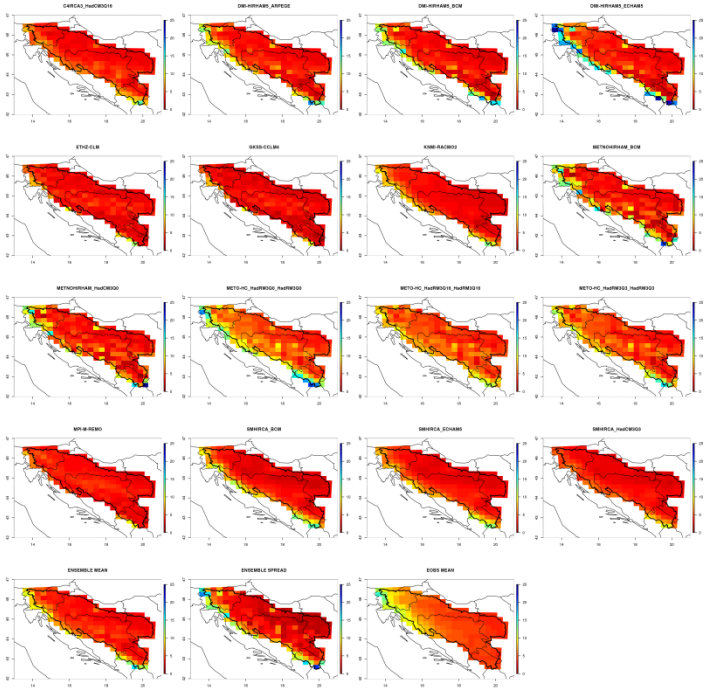

Figure 5: Mean daily precipitation on a wet day in winter for the validation period 1991-2010. Shown are raw simulations with 16 different climate model runs (see table 2 for details), ensemble mean, ensemble spread and observed mean (EOBS MEAN). Unit on all images is mm/day.

Figures 2–5 represent daily mean precipitation values on wet days (when daily precipitation exceeds 0.1 mm) from raw climate model runs. Means were calculated for each season. Each figure shows mean daily precipitation for 16 climate model runs as well as the observational mean for visual comparison. Ensemble spread represents the difference between maximum and minimum model simulations for each grid cell; this measure therefore indicates regions, where the largest differences occur between model simulations.

In general, we can observe that raw model simulations underestimate the mean daily precipitation all over the domain. The highest deviations can be observed in the north-western part of the Sava river basin, where also the highest mean daily precipitation occurs. The ensemble spread indicates that the highest difference between models occurs in the north-western part of the domain (including the Julian Alps, Dinaric Alps and Kamniško-Savinjske Alps in Slovenia) and along the Dinaric Alps towards the south-eastern part of the basin. Highly complex orography prevails along that region, which influences precipitation occurrence and intensity in all seasons. Moreover, orography can locally significantly influence climate features of the region, which cannot be resolved in climate model simulations due to the limited resolution. The ensemble mean (mean of 16 ensemble members) tends to underestimate daily precipitation as well, since all ensemble members systematically underestimate the mean daily precipitation. The highest deviations between simulated and observed precipitation generally occur in autumn.

Similar spatial patterns can be observed for seasonal precipitation (***Figures 6–9***). Models in general correctly reproduce the east-west decreasing precipitation trend over the basin; however, significant differences occur between them. A model comparison reveals that the models generally underestimate precipitation in autumn and summer in the north-eastern part of the basin. Seasonal precipitation is spatially highly variable, which is not the case with the E-OBS data. The highest ensemble spread can be seen over complex orography (western border of the basin), which was also the case with simulated daily precipitation. The ensemble mean most closely resembles the observed values in all seasons, especially regarding the spatial precipitation variability. Models in general overestimate precipitation in winter and spring. According to the simulation of mean daily precipitation intensity on wet days in these seasons (it was underestimated), we can conclude that the number of wet days in raw climate model simulations was overestimated.

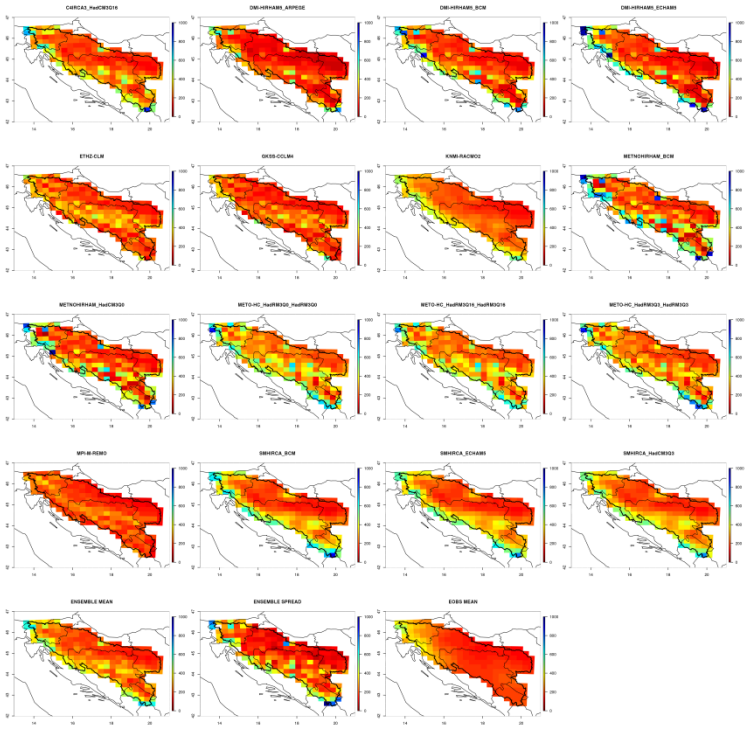

Figure 6: Mean seasonal precipitation for spring for the validation period 1991-2010. Shown are raw simulations with 16 different climate model runs (see table 2 for details), ensemble mean, ensemble spread and observed mean (EOBS MEAN). Unit on all images is mm.

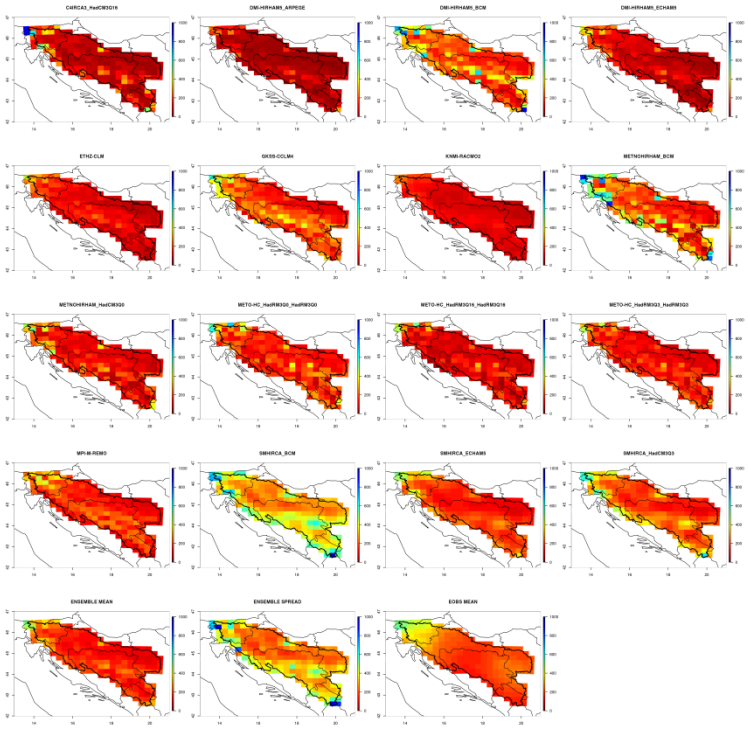

Figure 7: Mean seasonal precipitation for sumer for the validation period 1991-2010. Shown are raw simulations with 16 different climate model runs (see table 2 for details), ensemble mean, ensemble spread and observed mean (EOBS MEAN). Unit on all images is mm.

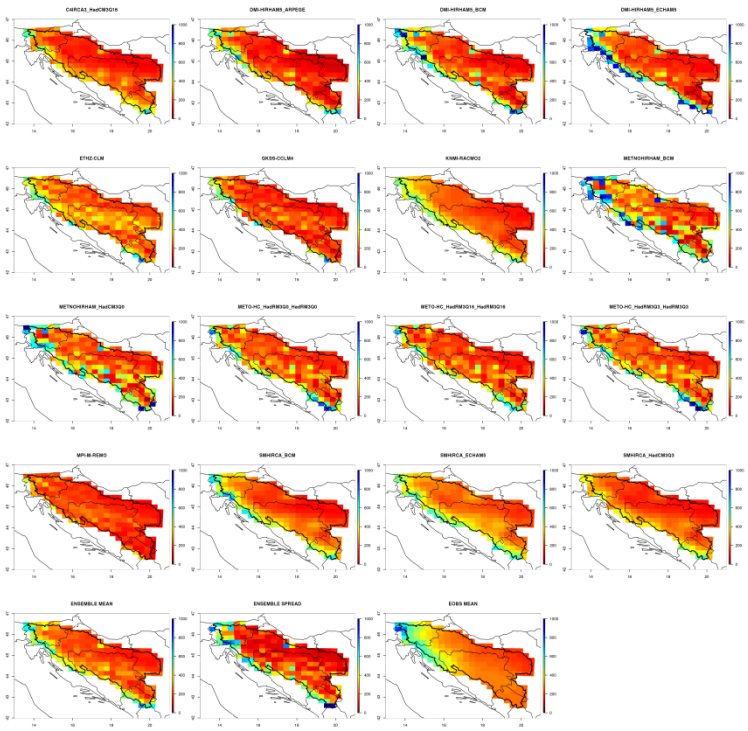

Figure 8: Mean seasonal precipitation for autumn for the validation period 1991-2010. Shown are raw simulations with 16 different climate model runs (see table 2 for details), ensemble mean, ensemble spread and observed mean (EOBS MEAN). Unit on all images is mm.

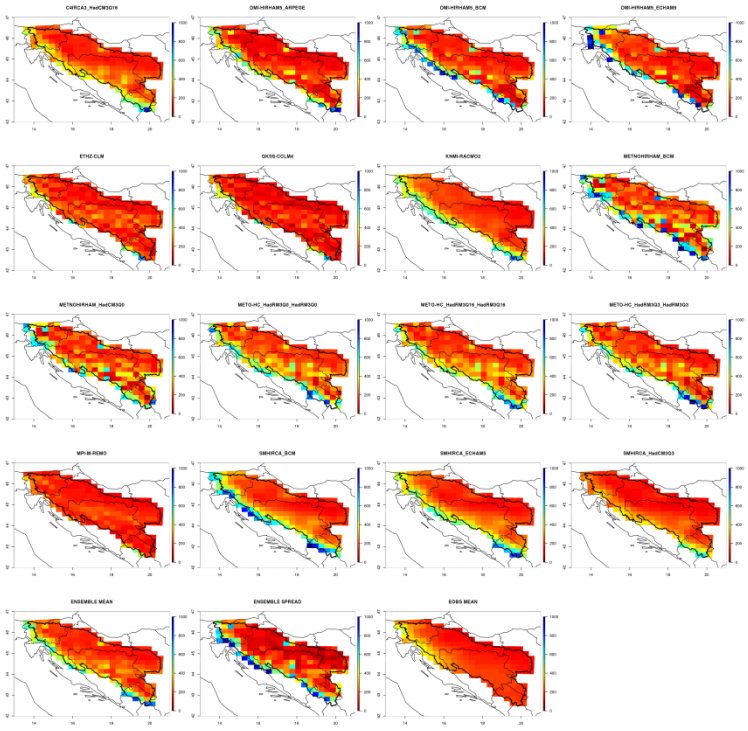

Figure 9: Mean seasonal precipitation for winter for the validation period 1991-2010. Shown are raw simulations with 16 different climate model runs (see table 2 for details), ensemble mean, ensemble spread and observed mean (EOBS MEAN). Unit on all images is mm.

Figures 10–14 show PSS for the validation period 1991–2010. The quality of simulated precipitation is spatially and model dependent. In spring, the lowest PSS of raw model simulations occurs in north-western part (Slovenia) and southern part of the basin, where also the most complex orography prevails. PSS is significantly lower in the summer all over the basin. This is expected, since local convection is a primary cause of precipitation. In autumn and winter, better quality of raw simulations can be observed, especially in the eastern part of the basin (***Figures 12 and 14***). This is expected, since mainly large-scale precipitation events occur over the area in these seasons, which is better simulated than the convective precipitation in summer.

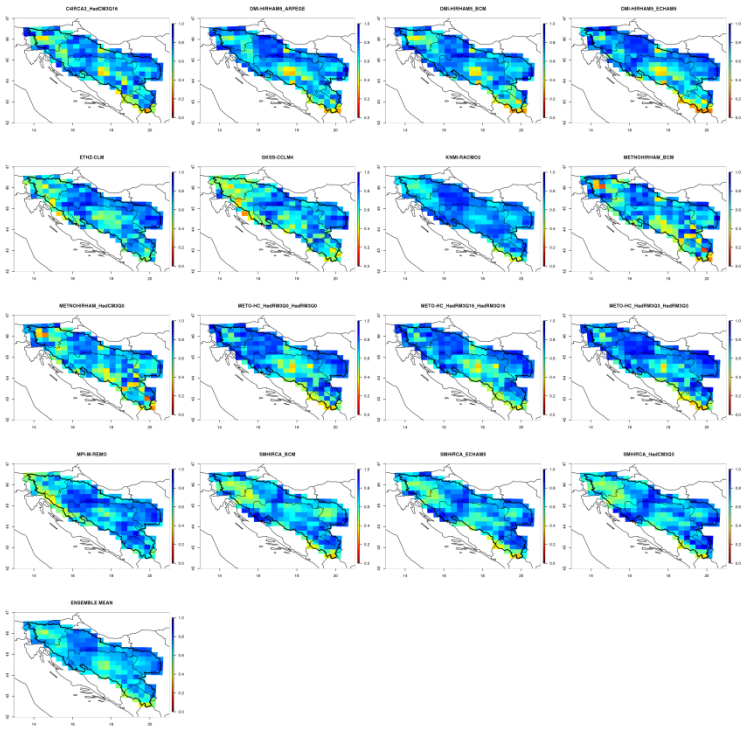

Figure 10: Perkins Skill Score for raw simulations of daily precipitation in spring for the validation period 1991-2010. Shown is PSS for 16 different climate model runs (see table 2 for details) and ensemble mean.

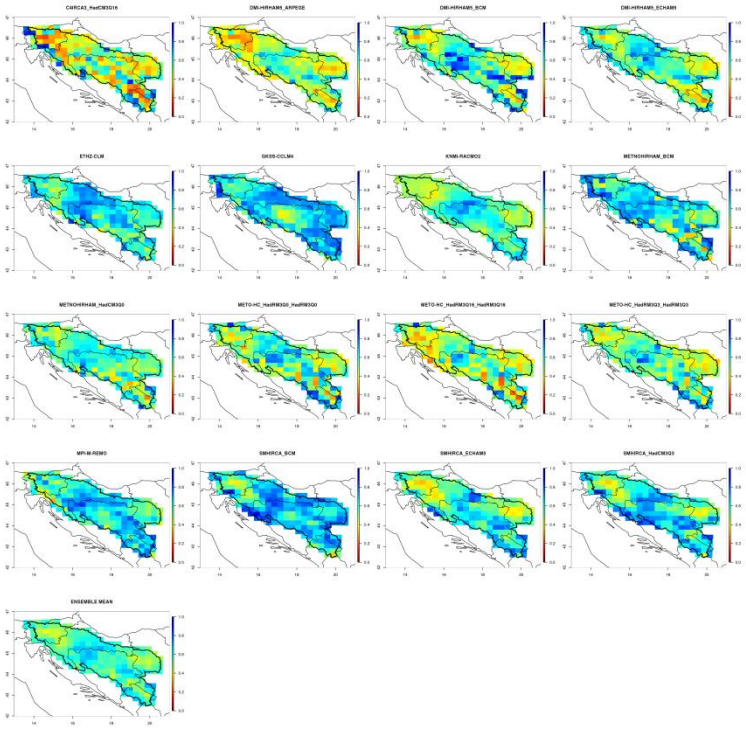

Figure 11: Perkins Skill Score for raw simulations of daily precipitation in summer for the validation period 1991-2010. Shown is PSS for 16 different climate model runs (see table 2 for details) and ensemble mean.

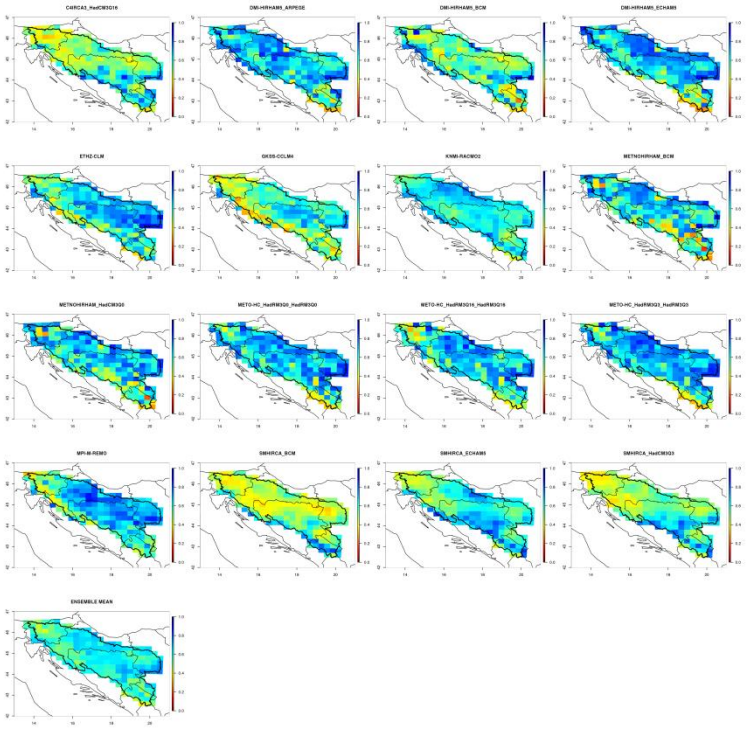

Figure 12: Perkins Skill Score for raw simulations of daily precipitation in autumn for the validation period 1991-2010. Shown is PSS for 16 different climate model runs (see table 2 for details) and ensemble mean.

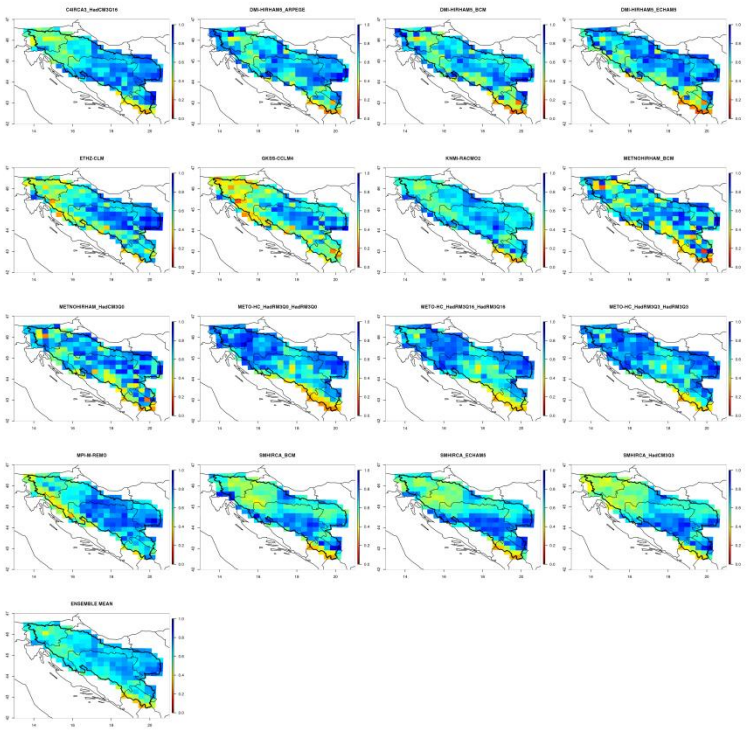

Figure 13: Perkins Skill Score for raw simulations of daily precipitation in winter for the validation period 1991-2010. Shown is PSS for 16 different climate model runs (see table 2 for details) and ensemble mean.

The bias corrected precipitation shows lower deviations from the observed data for daily as well as seasonal precipitation. ***Figures 15–19*** show spatial differences between PSS of bias corrected and raw climate model simulations for the validation period. Positive values therefore indicate an improvement in the quality of simulations of daily precipitation, whereas negative values represent a lower quality of bias corrected simulations.

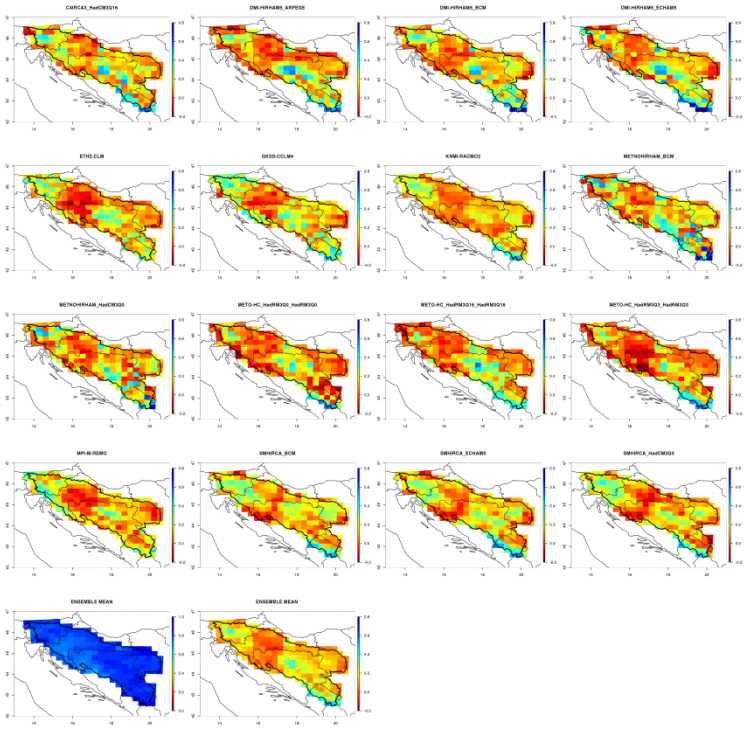

Figure 14: Perkins Skill Score for bias corrected simulations of daily precipitation in spring for the validation period 1991-2010. Shown are differences between PSS for bias corrected simulations and PSS for raw simulations (positive values therefore represent improvement in simulation quality) for 16 different climate model runs (see table 2 for details). In the bottom, ensemble mean PSS for bias corrected daily precipitation and ensemble mean for PSS differences are shown. The later indicates spatial distribution of quality improvement after bias correction across the Sava river basin.

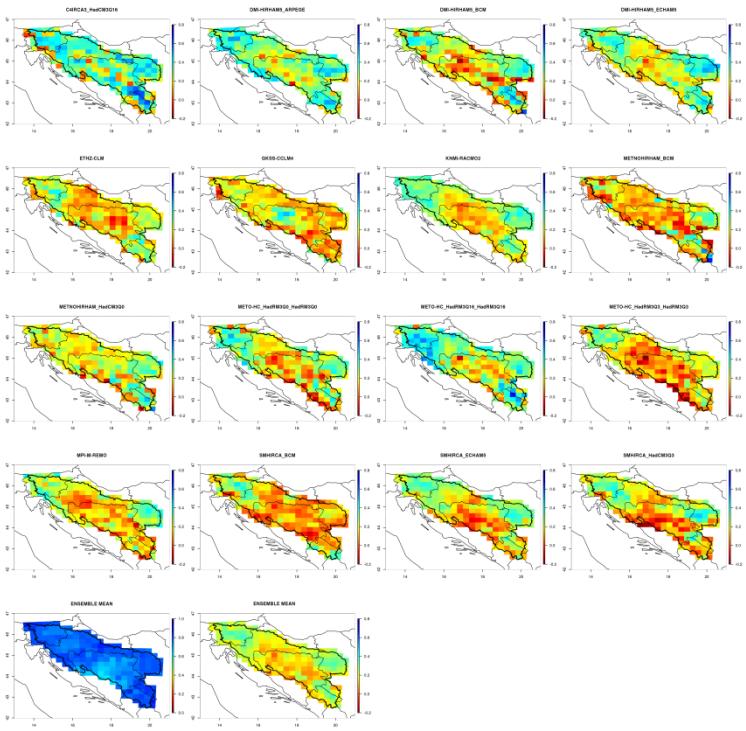

Figure 15: Perkins Skill Score for bias corrected simulations of daily precipitation in summer for the validation period 1991-2010.

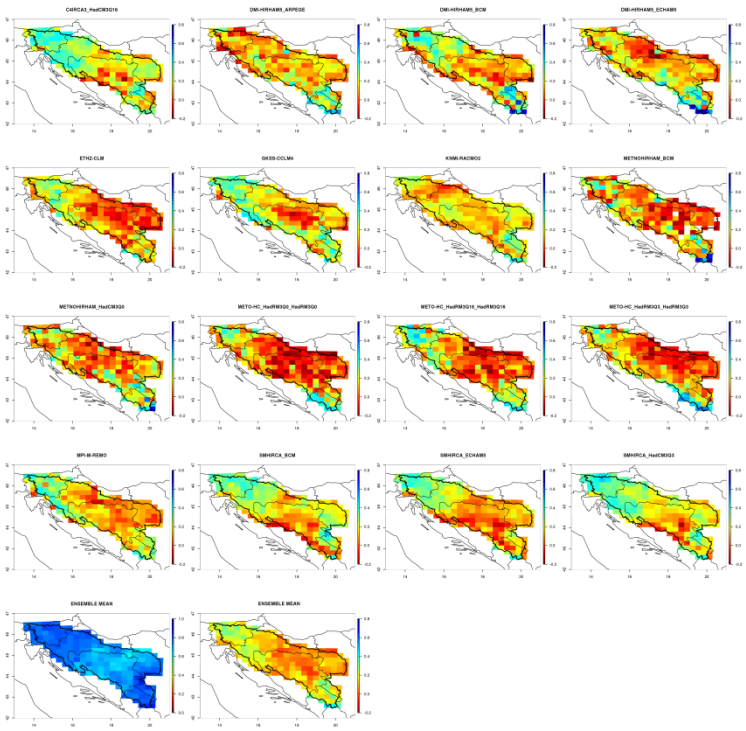

Figure 16: Perkins Skill Score for bias corrected simulations of daily precipitation in autumn for the validation period 1991-2010.

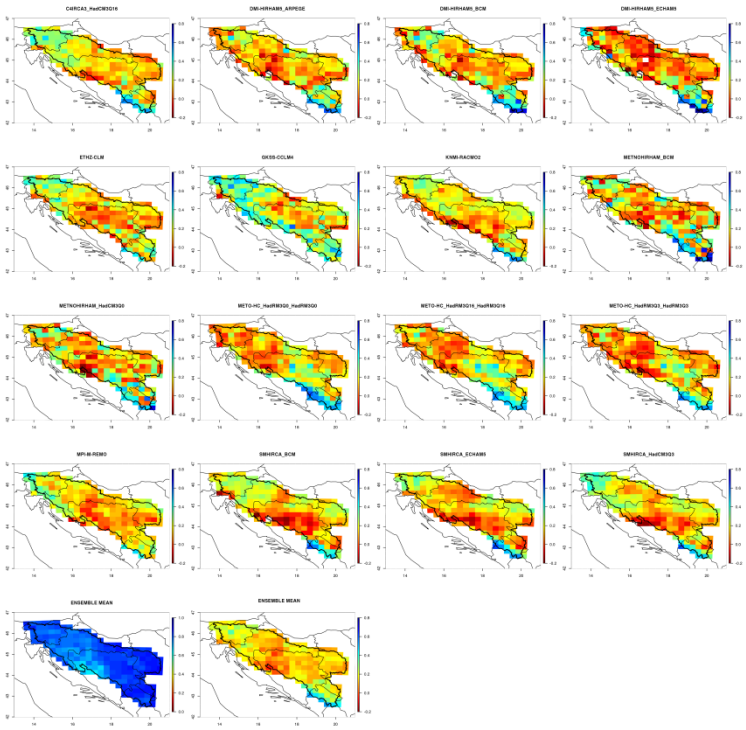

Figure 17: Perkins Skill Score for bias corrected simulations of daily precipitation in winter for the validation period 1991-2010.

For spring daily precipitation intensity, we can, in general, observe increased quality of bias corrected simulations in north-western part of the basin (Slovenian territory), especially in south-eastern and eastern parts of the basin. Very little improvement can be observed for the central part of the basin (border between Croatia and Bosnia and

Herzegovina). Looking at each model, we can see a slight quality deterioration of bias corrected simulations in comparison to raw simulations, but these are very rare. Therefore, we can conclude that the bias correction procedure significantly improved precipitation simulations on the basin level. The quality of bias corrected summer precipitation improved significantly in comparison to raw climate model simulations. Similarly to spring precipitation, the improvement was better in the north-western and south-eastern parts of the basin, whereas aslightly lower improvement can be seen for the central part of the basin. A similar pattern can be observed for the autumn daily precipitation intensity; however, in autumn the improvement of quality was slightly lower over the basin than in summer. Lower quality of simulations can be observed over few grid points in the central part of the basin for three versions of the Hadley RCM (HadRM3Q0, HadRM3Q3 and HadRM3Q16). Nevertheless, the quality improved over the greater part of the basin. In winter, bias correction generally improved the quality of model simulations over the basin, where the same patterns of improvement can be observed as those in other seasons. A slight deterioration of quality can be observed over the mountainous part of Bosnia and Herzegovina.

We can conclude that the bias correction procedure improved the quality of model simulations over the basin, except over the central part of Bosnia and Herzegovina. This could be related to the stationarity of the bias correction procedure; this is the main assumption stating that the transfer function does not change in future climate. This assumption could be violated in the central part of Bosnia and Herzegovina, where the lowest improvement or slight worsening of the quality of simulations was obtained after bias correction. Another possible reason for the low degree of improvement could be in the simulations of climate models (large scale as well as convective precipitation). Climate models should therefore be verified for simulation of large scale weather patterns, causing precipitation in this area, but this is out of the scope of this study.

Since bias correction generally improved the quality of precipitation simulations over the Sava river basin, it was applied to raw climate model simulations for the 21st Century.

4.2 VALIDATION OF TEMPERATURE SIMULATIONS

Bias correction has been applied to raw temperature simulations as well. In the first step, the validation of corrected climate model simulations is presented. For each season, mean temperature was calculated from raw climate model simulations and compared to bias corrected values. The comparison was done for the validation period 1991–2010, where bias corrected values were calculated based on transfer functions from the period 1961–1990. PSS was used as the model performance measure.

The quality of temperature simulations generally improved in spring, summer and autumn, whereas in winter there were no significant differences across the basin (***Figures 18–21***). In spring, summer and autumn, the highest degree of improvement can be seen for the area with a complex orography (north-western part and western border of the basin). The highest improvement in quality can be observed for summer; this is expected, since local orography features influence convection occurrence and therefore also temperature distribution. In winter, no significant differences can be observed between bias corrected and raw climate model simulations. There are, however, significant differences in quality improvement or deterioration between

different model runs. Bias correction of RCMs that were nested within Hadley GCM, showed no improvement or , indeed, evena a slight deterioration in the simulation quality.

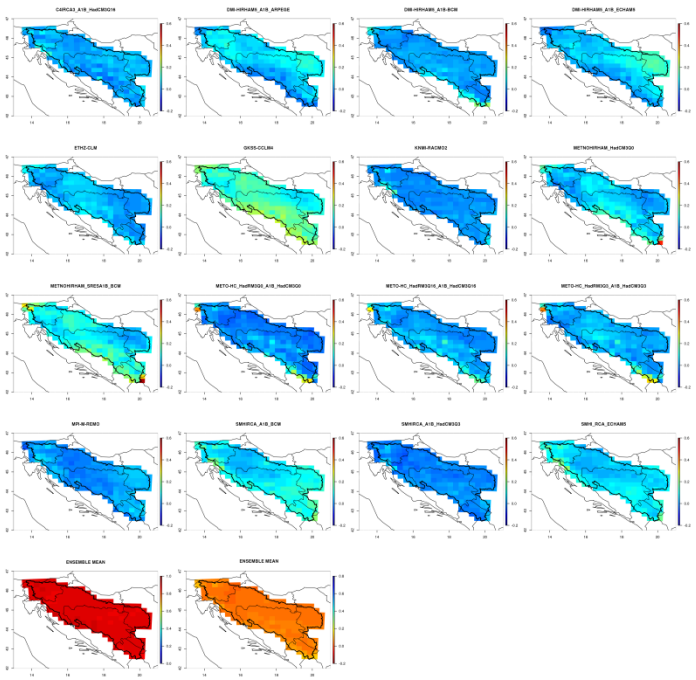

Figure 18: Perkins Skill Score for bias corrected simulations of daily temperature in spring for the validation period 1991-2010. Shown are differences between PSS for bias corrected simulations and PSS for raw simulations (positive values therefore represent improvement in simulation quality) for 16 different climate model runs (see table 2 for details). In the bottom, ensemble mean PSS for bias corrected daily temperature and ensemble mean for PSS differences are shown. The later indicates spatial distribution of quality improvement after bias correction across the Sava river basin.

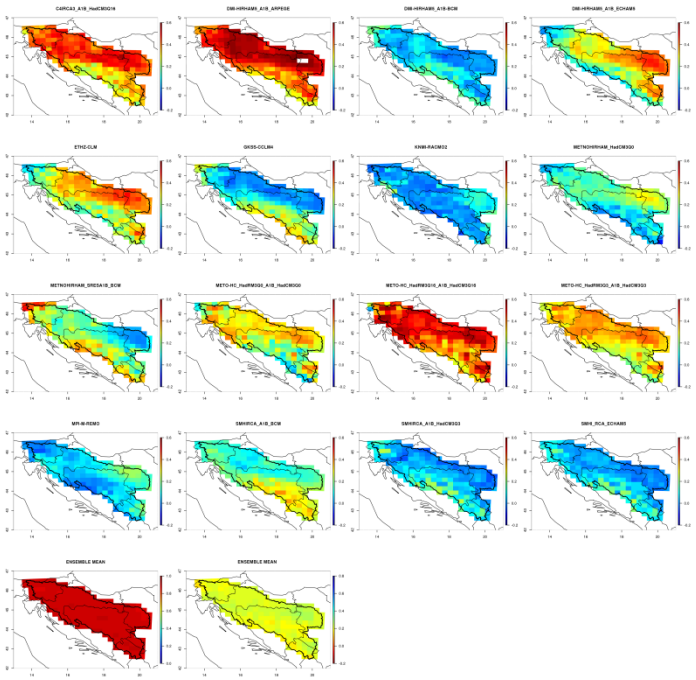

Figure 19: Perkins Skill Score for bias corrected simulations of daily temperature in summer for the validation period 1991-2010.

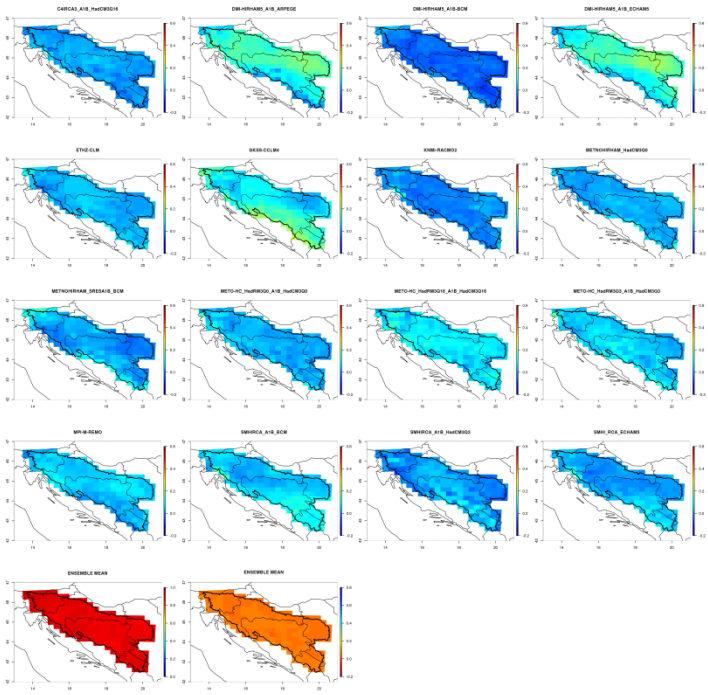

Figure 20: Perkins Skill Score for bias corrected simulations of daily temperature in autumn for the validation period 1991-2010.

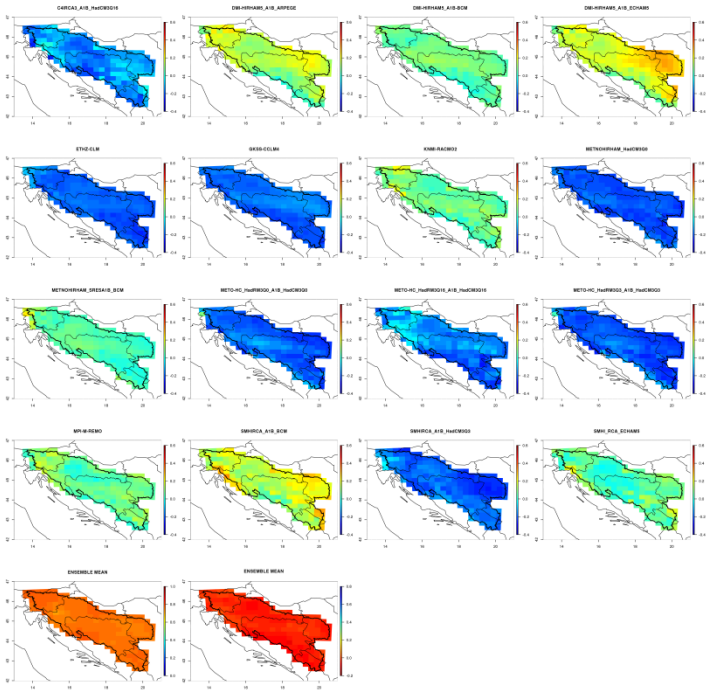

Figure 21: Perkins Skill Score for bias corrected simulations of daily temperature in winter for the validation period 1991-2010.

4.3 CLIMATE PROJECTIONS

4.3.1 SEASONAL PRECIPITATION

Projections of seasonal precipitation were made for three future periods: 2011–2040 (P1), 2041–2070 (P2) and 2071–2100 (P3). ***Figures 22–24*** show seasonal changes in precipitation during the three periods. Shown are ensemble mean changes (absolute and relative changes according to the reference period). Grid points, where at least 80% of the models agree in the sign of change relative to the reference period, are marked with black dots. All projections were made using bias corrected precipitation simulations, where transfer functions were calibrated for the period 1961–2000. Standard deviation was calculated to characterize precipitation interannual variability.

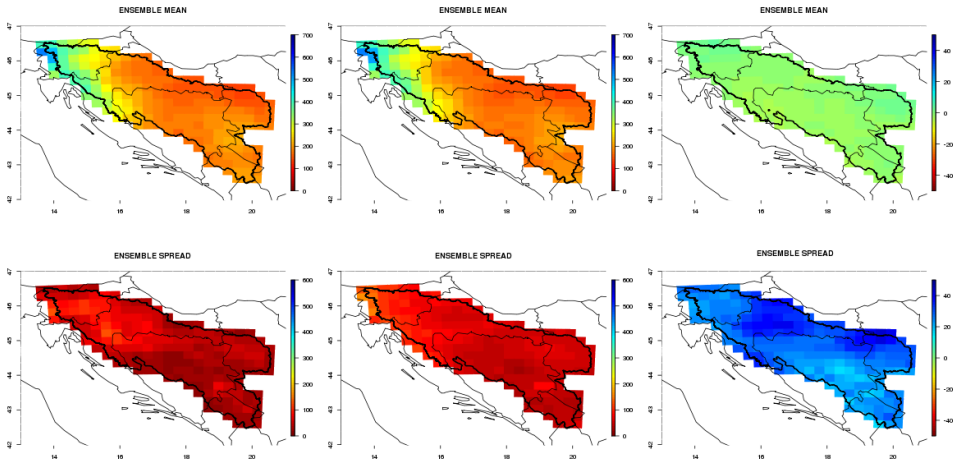

Figure 22: Projections of spring precipitation. Shown are: ensemble mean and spread for the reference period (left column, units is mm/day), ensemble mean and spread for 2011-2040 (middle column, unit is mm/day) and ensemble mean and spread of changes relative to the reference period (right column, unit is %). Locations, where at least 80 % of models agree on the sign of change are marked with black dot.

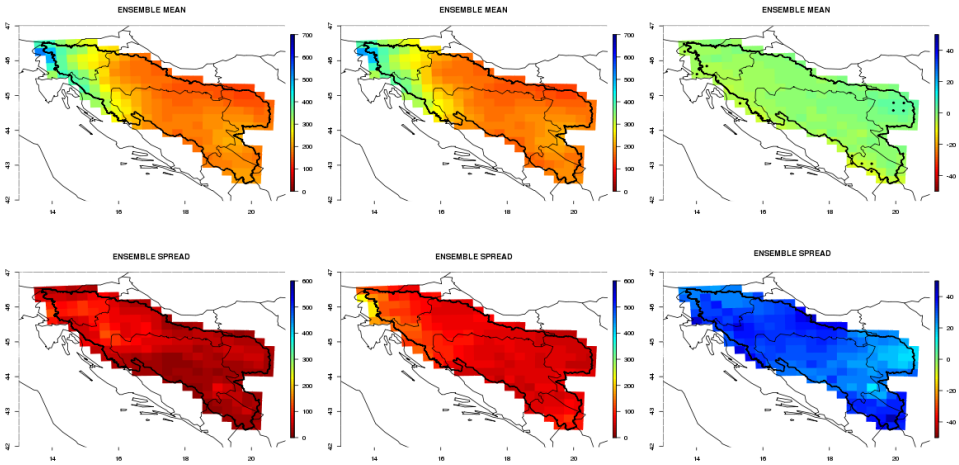

Figure 23: Projections of spring precipitation. Shown are: ensemble mean and spread for the reference period (left column, units is mm/day), ensemble mean and spread for 2041-2070 (middle column, unit is mm/day) and ensemble mean and spread of changes relative to the reference period (right column, unit is %). Locations, where at least 80 % of models agree on the sign of change are marked with black dot.

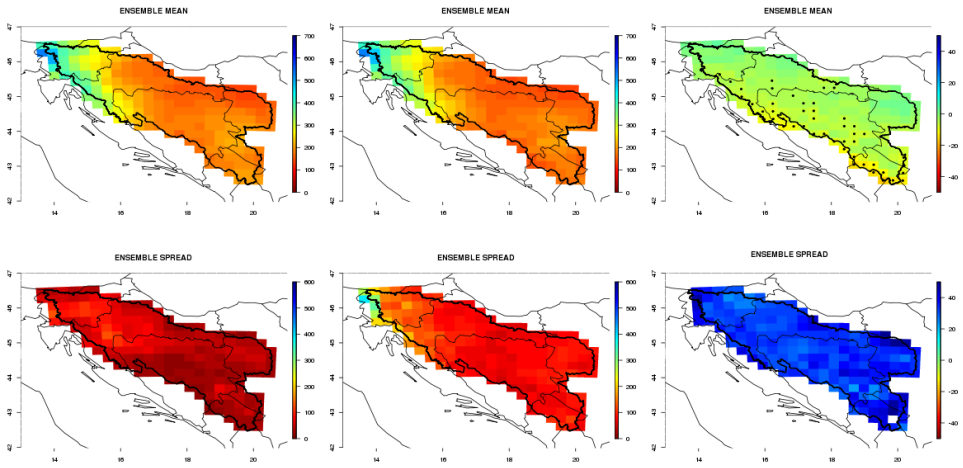

Figure 24: Projections of spring precipitation. Shown are: ensemble mean and spread for the reference period (left column, units is mm/day), ensemble mean and spread for 2071-2100 (middle column, unit is mm/day) and ensemble mean and spread of changes relative to the reference period (right column, unit is %). Locations, where at least 80 % of models agree on the sign of change are marked with black dot.

No significant changes are expected in spring during period P1. High regional differences, however, exist between model simulations. Highest ensemble spread of projected values can be observed in north-eastern part of the basin. Precipitation is expected to decrease in periods P2 and P3 in the south-western part (between 10 % and 15 %), where models generally agree in the sign of change. Slight, but uncertain increase is expected in the northern and eastern parts of the basin. Precipitation variability is expected to increase in the central part (southern Croatia and Bosnia and Herzegovina) and south-western part of the basin, i.e. up to 30 % towards the end of the 21st Century. Models disagree in the sign of change in other parts of the basin. Highest model spread in precipitation variability can be observed in the north-western mountainous part of Slovenia.

Precipitation changes are more pronounced in the summer (***Figures 25-27***). Precipitation is expected to decrease by 10 % in the south-eastern part of the basin during period P1. A high ensemble spread can be observed for the same period in parts of central Slovenia, where the sign of change is uncertain. All models agree in the sign of change over the whole basin in periods P2 and P3. In period P2, precipitation is expected to decrease between 10 % in the north-western part and 20 % in the south-eastern part of the basin. A similar change pattern can be observed for period P3, where precipitation is expected to decrease between 20 % in the north-western part and 40 % in the south-eastern part of the basin. All models agree in the sign of change, even though that the high ensemble spread can be observed in the north-western part of the basin. Seasonal precipitation variability is expected to decrease throughout the 21st Century. Small changes are expected for period P1 with disagreeing model simulations over the basin (especially central part of the basin, where models simulate changes from an increase of variability by 40 % to a decrease of variability by 40 %). A more stable signal can be observed for periods P2 and P3, where a decrease of summer precipitation variability is expected.

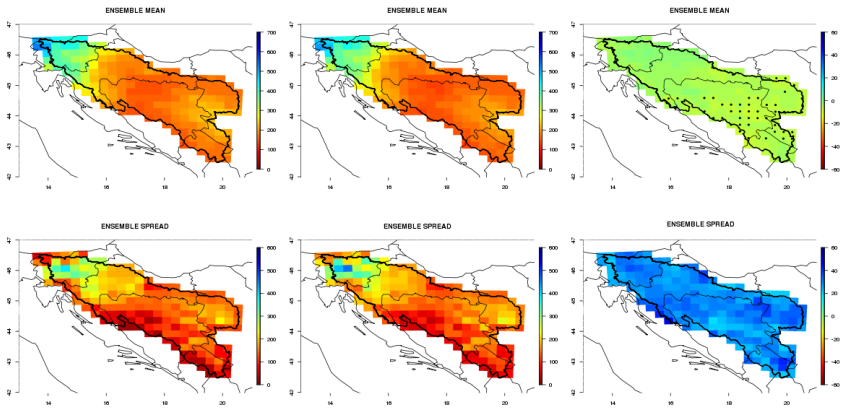

Figure 25: Projections of summer precipitation. Shown are: ensemble mean and spread for the reference period (left column, unit is mm/day), ensemble mean and spread for 2011-2040 (middle column, unit is mm/day) and ensemble mean and spread of changes relative to the reference period (right column, unit is %). Locations, where at least 80 % of models agree on the sign of change are marked with black dot.

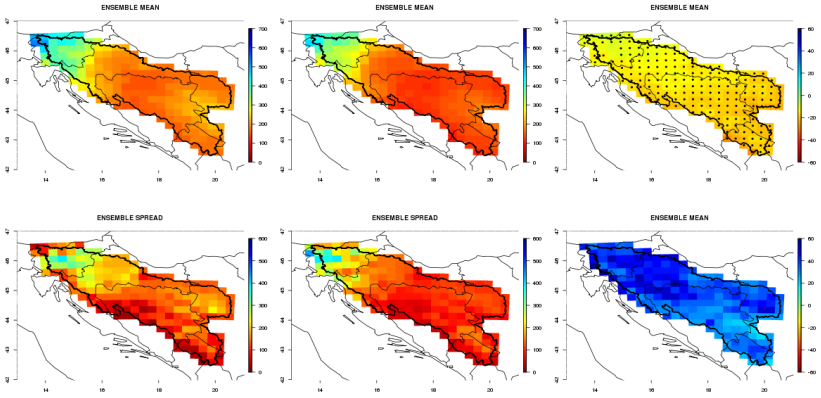

Figure 26: Projections of summer precipitation. Shown are: ensemble mean and spread for the reference period (left column, unit is mm/day), ensemble mean and spread for 2041-2070 (middle column, unit is mm/day) and ensemble mean and spread of changes relative to the reference period (right column, unit is %). Locations, where at least 80 % of models agree on the sign of change are marked with black dot.

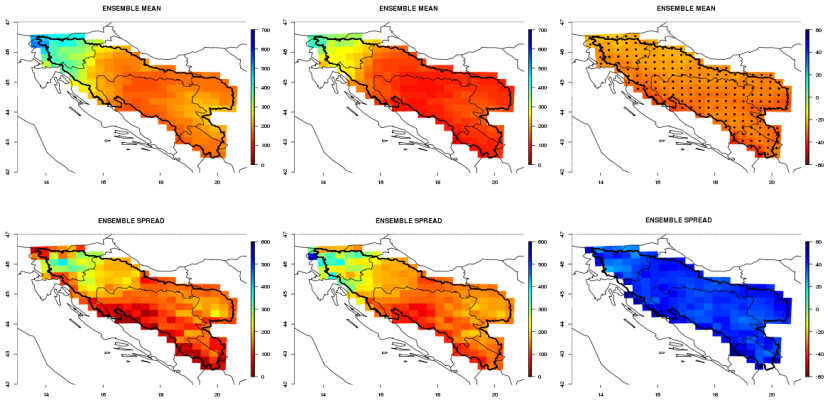

Figure 27: Projections of summer precipitation. Shown are: ensemble mean and spread for the reference period (left column, unit is mm/day), ensemble mean and spread for 2071-2100 (middle column, unit is mm/day) and ensemble mean and spread of changes relative to the reference period (right column, unit is %). Locations, where at least 80 % of models agree on the sign of change are marked with black dot.

In autumn, non-significant changes in seasonal precipitation are expected over the basin in period P1 (***Figures 28–30***). Precipitation is expected to increase in the north-western and south-eastern parts in period P2 (around 10 %). Towards the end of the century, a slight decrease is expected in the south-western part, whereas a non-significant increase is expected in the northern part of the basin. The highest model spread can again be observed in the north-eastern part of the basin. A high ensemble spread can be observed in the changes of seasonal precipitation variability as well. In autumn, the variability is expected to increase during the 21st Century, especially in north-western and south eastern parts of the basin. The expected increase is around 10 % in period P1, 20 % in period P2 and 30 % in period P3. In Croatia and northern part of Bosnia and Herzegovina, changes in precipitation variability are non-significant throughout the 21st Century.

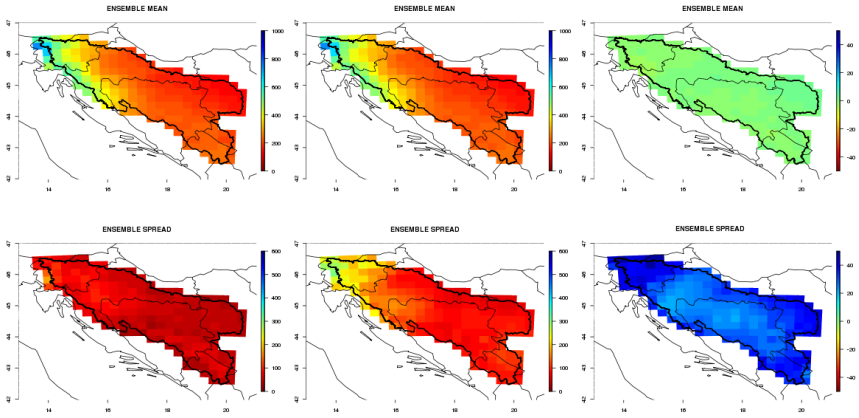

Figure 28: Projections of autumn precipitation. Shown are: ensemble mean and spread for the reference period (left column, unit is mm/day), ensemble mean and spread for 2011-2040 (middle column, unit is mm/day) and ensemble mean and spread of changes relative to the reference period (right column, unit is %). Locations, where at least 80 % of models agree on the sign of change are marked with black dot.

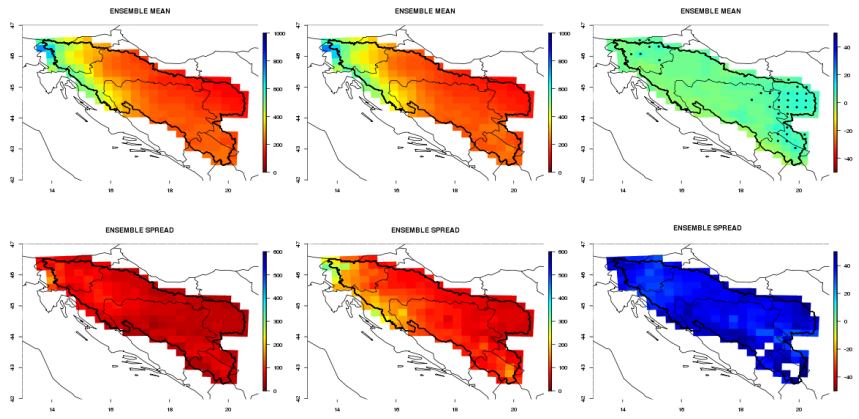

Figure 29: Projections of autumn precipitation. Shown are: ensemble mean and spread for the reference period (left column, unit is mm/day), ensemble mean and spread for 2041-2070 (middle column, unit is mm/day) and ensemble mean and spread of changes relative to the reference period (right column, unit is %). Locations, where at least 80 % of models agree on the sign of change are marked with black dot.

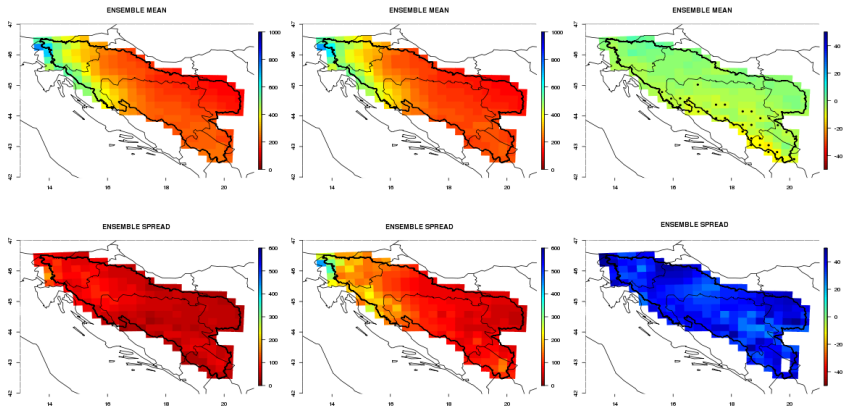

Figure 30: Projections of autumn precipitation. Shown are: ensemble mean and spread for the reference period (left column, unit is mm/day), ensemble mean and spread for 2071-2100 (middle column, unit is mm/day) and ensemble mean and spread of changes relative to the reference period (right column, unit is %). Locations, where at least 80 % of models agree on the sign of change are marked with black dot.

In winter (***Figures 31–33***), precipitation is expected to increase during the 21st Century, especially in the north-western part of the basin (around 10 % in period P1, 20 % in period P2 and 30 % in period P3). Non-significant changes are expected in precipitation variability in period P1; the model spread, however, is very high. In periods P2 and P3, a significant increase of variability up to 40 % is expected over the basin (models also agree in the sign of change).

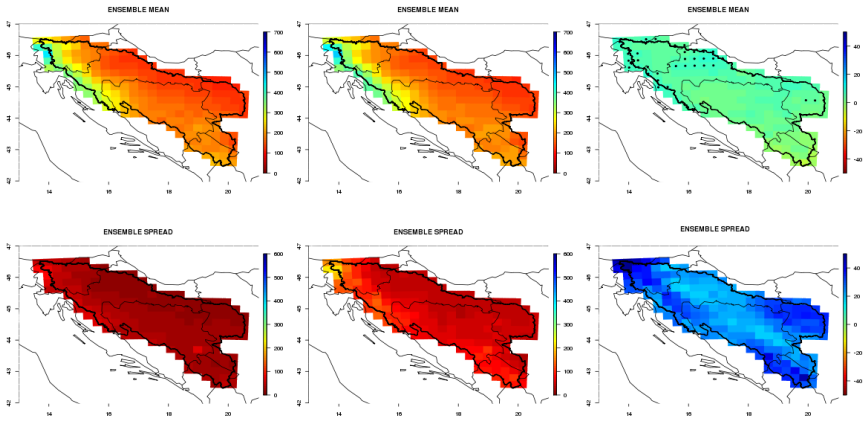

Figure 31: Projections of winter precipitation. Shown are: ensemble mean and spread for the reference period (left column, unit is mm/day), ensemble mean and spread for 2011-2040 (middle column, unit is mm/day) and ensemble mean and spread of changes relative to the reference period (right column, unit is %). Locations, where at least 80 % of models agree on the sign of change are marked with black dot.

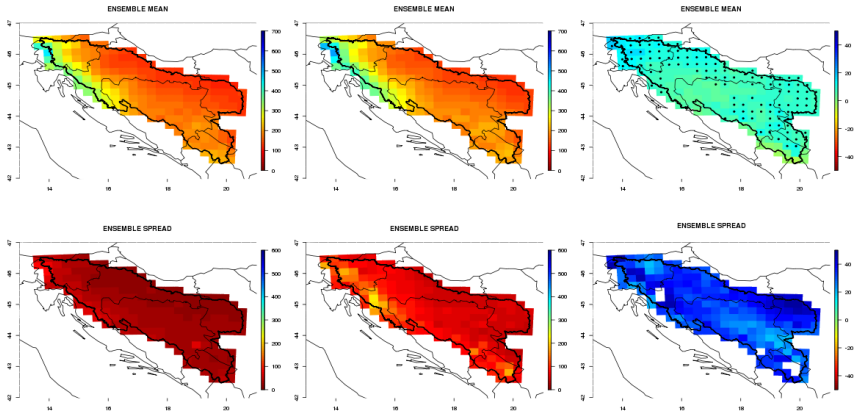

Figure 32: Projections of winter precipitation. Shown are: ensemble mean and spread for the reference period (left column, unit is mm/day), ensemble mean and spread for 2041-2070 (middle column, unit is mm/day) and ensemble mean and spread of changes relative to the reference period (right column, unit is %). Locations, where at least 80 % of models agree on the sign of change are marked with black dot.

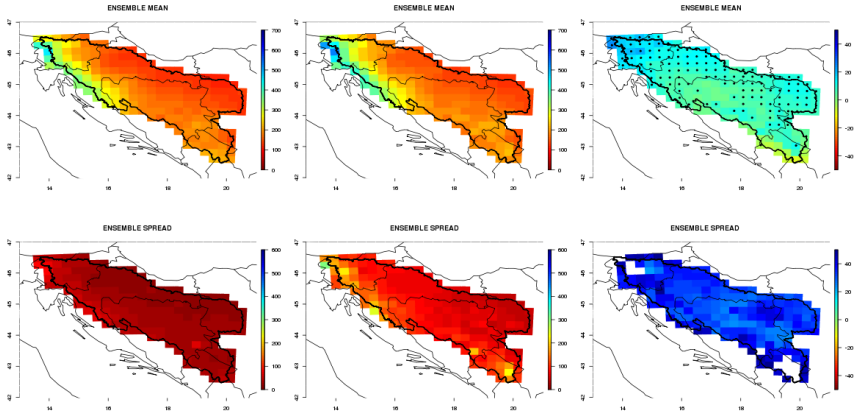

Figure 33: Projections of winter precipitation. Shown are: ensemble mean and spread for the reference period (left column, unit is mm/day), ensemble mean and spread for 2071-2100 (middle column, unit is mm/day) and ensemble mean and spread of changes relative to the reference period (right column, unit is %). Locations, where at least 80 % of models agree on the sign of change are marked with black dot.

4.3.2 EXTREME DAILY PRECIPITATION INDICES

Several indices were calculated, describing extreme precipitation events:

a) 95^{th} percentile of daily seasonal precipitation
b) interannual mean of maximum 24-hour precipitation
c) interannual mean of maximum 48-hour precipitation
d) daily precipitation intensity with a return period of 20 years
e) daily precipitation intensity with a return period of 100 years

For the above mentioned indicators, absolute values were calculated for three future periods (P1, P2 and P3) as well as changes relative to the reference period. Precipitation intensities with the two return periods were calculated based on maximum-likelihood fitting for the generalized extreme value distribution of maximum daily precipitation (Gilleland et al., 2006). ***Figures 34–53*** show spatial distribution of ensemble mean as well as E-OBS mean values of selected indicators of extreme precipitation for the reference period 1971–2000.

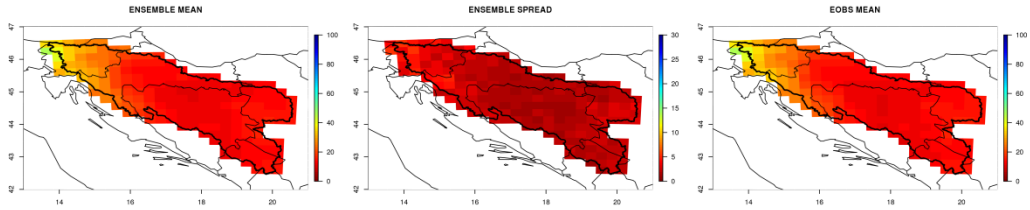

Figure 34: Ensemble mean, spread (from 16 different model runs) and observed values for 95th percentile of spring daily precipitation for the reference period (1971-2000). Unit on all images is mm.

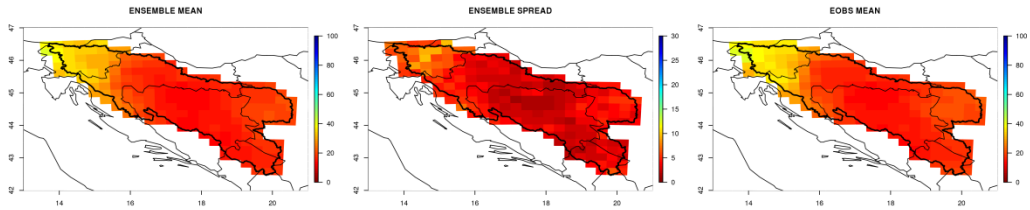

Figure 35: Ensemble mean, spread (from 16 different model runs) and observed values for 95th percentile of summer daily precipitation for the reference period (1971-2000). Unit on all images is mm.

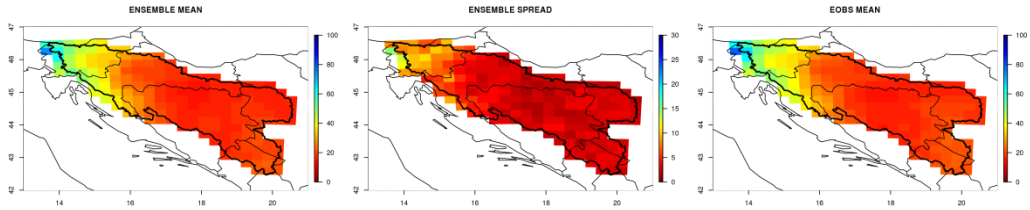

Figure 36: Ensemble mean, spread (from 16 different model runs) and observed values for 95th percentile of autumn daily precipitation for the reference period (1971-2000). Unit on all images is mm.

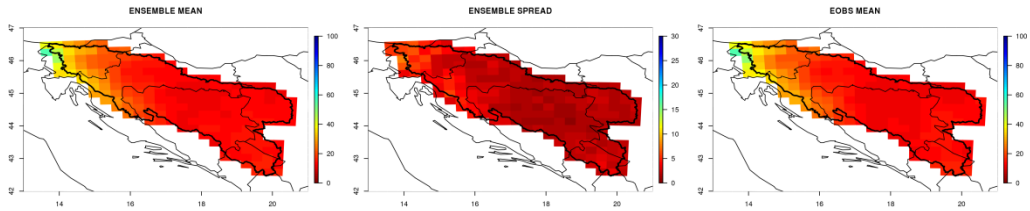

Figure 37: Ensemble mean, spread (from 16 different model runs) and observed values for 95th percentile of winter daily precipitation for the reference period (1971-2000). Unit on all images is mm.

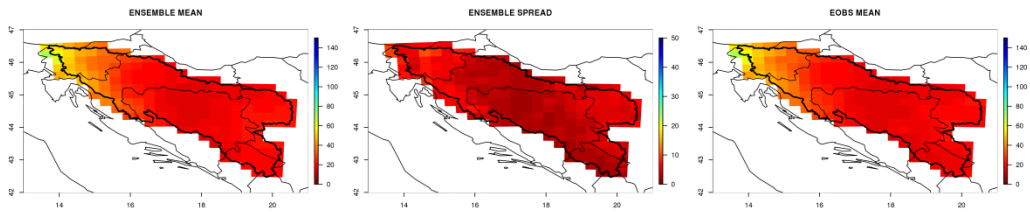

Figure 38: Ensemble mean, spread (from 16 different model runs) and observed values for 24 hours precipitation in spring for the reference period (1971-2000). Unit on all images is mm.

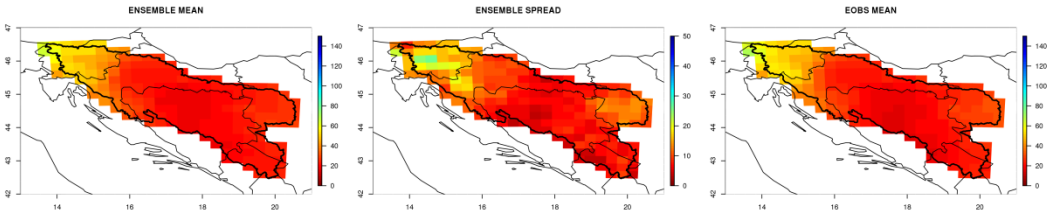

Figure 39: Ensemble mean, spread (from 16 different model runs) and observed values for 24 hours precipitation in summer for the reference period (1971-2000). Unit on all images is mm.

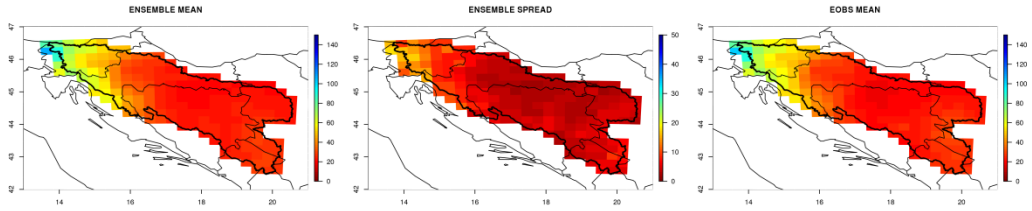

Figure 40: Ensemble mean, spread (from 16 different model runs) and observed values for 24 hours precipitation in autumn for the reference period (1971-2000). Unit on all images is mm.

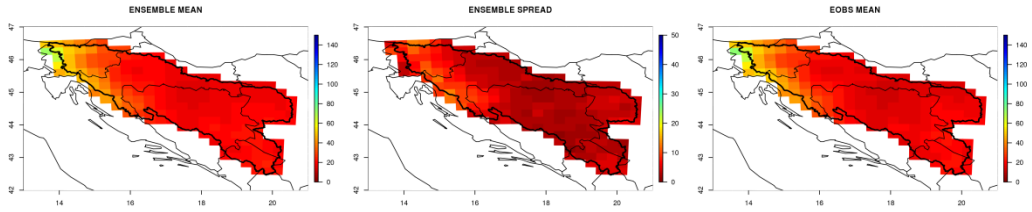

Figure 41: : Ensemble mean, spread (from 16 different model runs) and observed values for 24 hours precipitation in winter for the reference period (1971-2000). Unit on all images is mm.

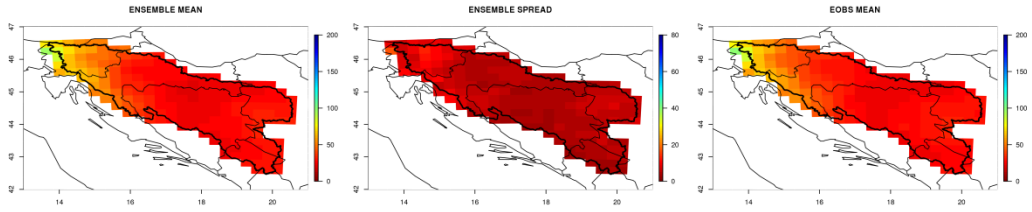

Figure 42: Ensemble mean, spread (from 16 different model runs) and observed values for 48 hours precipitation in spring for the reference period (1971-2000). Unit on all images is mm.

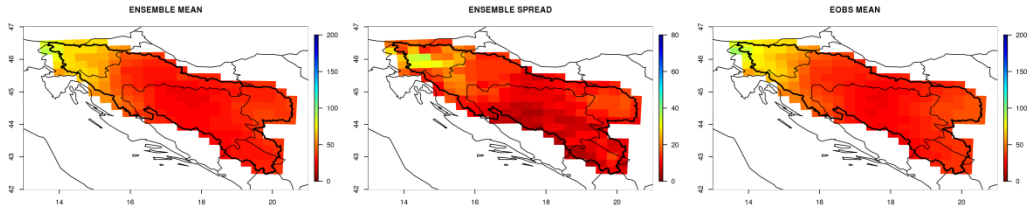

Figure 43: Ensemble mean, spread (from 16 different model runs) and observed values for 48 hours precipitation in summer for the reference period (1971-2000). Unit on all images is mm.

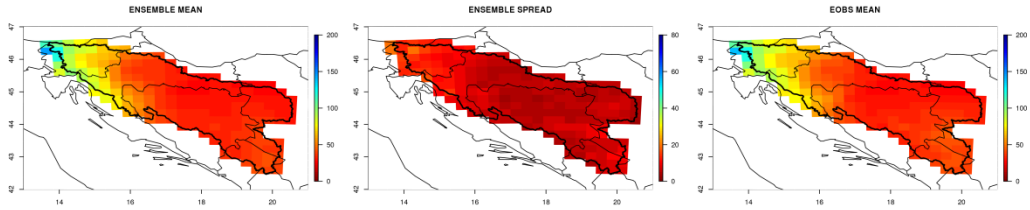

Figure 44: Ensemble mean, spread (from 16 different model runs) and observed values for 48 hours precipitation in autumn for the reference period (1971-2000). Unit on all images is mm.

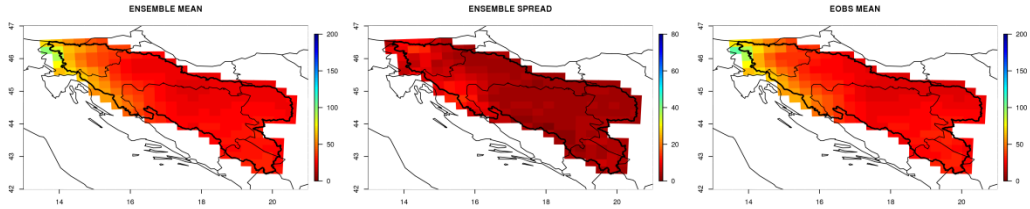

Figure 45: Ensemble mean, spread (from 16 different model runs) and observed values for 48 hours precipitation in winter for the reference period (1971-2000). Unit on all images is mm.

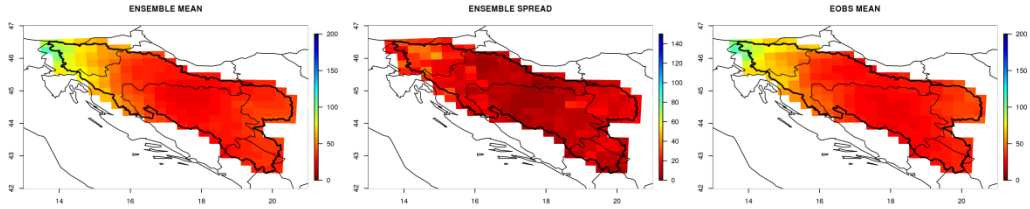

Figure 46: Ensemble mean, spread (from 16 different model runs) and observed values for spring daily precipitation intensity with return period 20 years for the reference period (1971-2000). Unit on all images is mm.

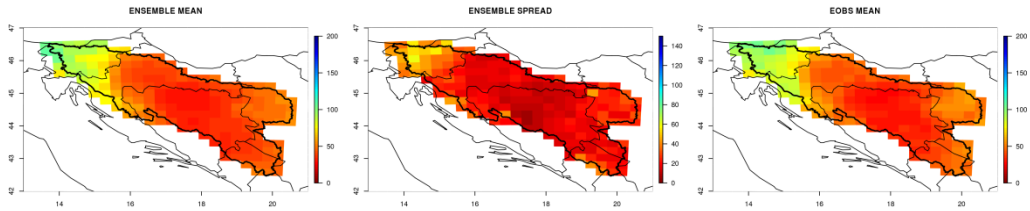

Figure 47: Ensemble mean, spread (from 16 different model runs) and observed values for summer daily precipitation intensity with return period 20 years for the reference period (1971-2000). Unit on all images is mm.

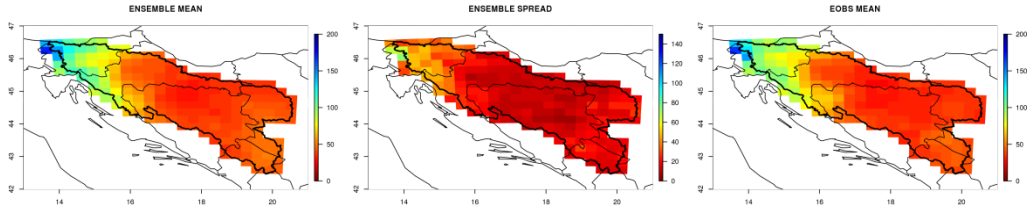

Figure 48: Ensemble mean, spread (from 16 different model runs) and observed values for autumn daily precipitation intensity with return period 20 years for the reference period (1971-2000). Unit on all images is mm.

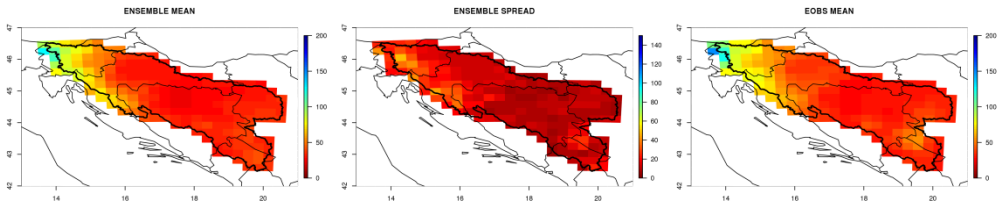

Figure 49: Ensemble mean, spread (from 16 different model runs) and observed values for winter daily precipitation intensity with return period 20 years for the reference period (1971-2000). Unit on all images is mm.

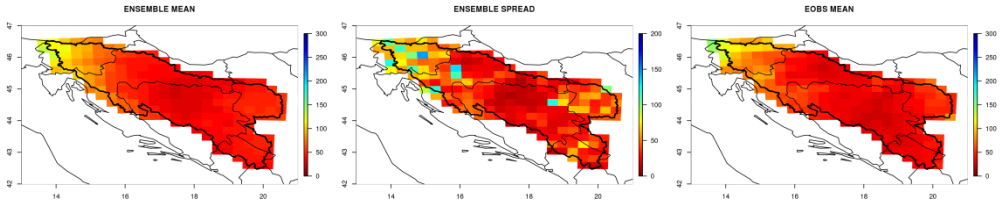

Figure 50: Ensemble mean, spread (from 16 different model runs) and observed values for spring daily precipitation intensity with return period 100 years for the reference period (1971-2000). Unit on all images is mm.

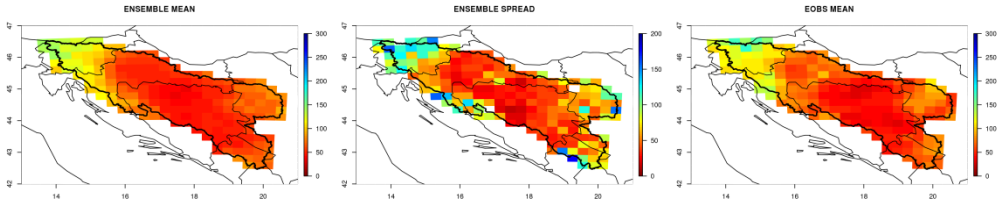

Figure 51: Ensemble mean, spread (from 16 different model runs) and observed values for summer daily precipitation intensity with return period 100 years for the reference period (1971-2000). Unit on all images is mm.

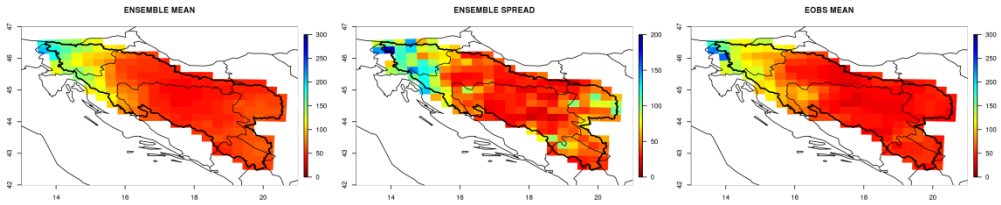

Figure 52: Ensemble mean, spread (from 16 different model runs) and observed values for autumn daily precipitation intensity with return period 100 years for the reference period (1971-2000). Unit on all images is mm.

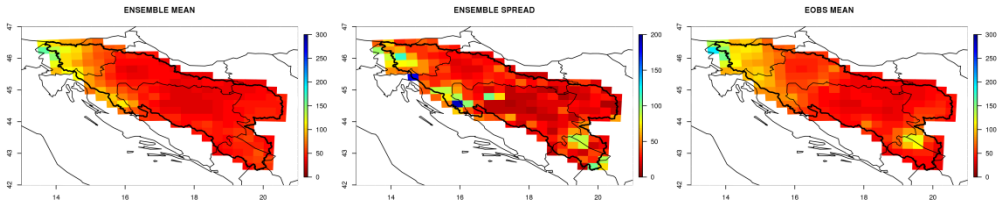

Figure 53: Ensemble mean, spread (from 16 different model runs) and observed values for winter daily precipitation intensity with return period 100 years for the reference period (1971-2000). Unit on all images is mm.

Figures 54–65 show the 95th percentiles of daily precipitation for each season. Each figure shows ensemble mean values for the reference period (1971–2000) and scenario periods (P1, P2 and P3) as well as relative changes according to the reference period. In spring, 95th percentile values ranged in the reference period from 80 mm in the north-western part of the basin, to 20 mm in central Bosnia. The 95th percentile of daily precipitation in spring is expected to increase throughout the 21st Century, when the ensemble mean indicates an increase of around 15 % in period P3 relative to the reference period. The change signal for 95th percentile of summer daily precipitation is less certain; it is expected to decrease in the western part of the basin towards the end of the century (approximately -10 %). The signal is less certain also in other parts of the basin, where models tend to disagree in the sign of change. There is an indication for an increase in the eastern part (***Figure 59***) of the basin (by approximately 10 % in the period P3). In autumn, 95th percentile of daily precipitation is expected to increase towards the end of the century. The change signal is very stable, since the majority of models agree also in the sign of change for the whole basin. The most pronounced increase can be observed in the eastern and northern parts of the basin (up to +30 % relative to the reference values). Similar change patterns are expected for winter, when the 95th percentile of daily precipitation increases (up to 30 % at the end of the century).

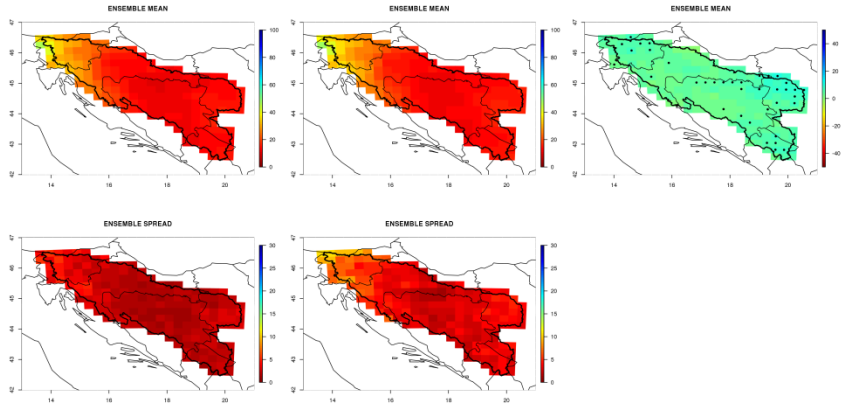

Figure 54: Projections for 95th percentile daily precipitation on wet day in spring. Shown are: ensemble mean and spread for the reference period (left column, unit is mm/day), ensemble mean and spread for 2011-2040 (middle column, unit is mm/day) and ensemble mean of changes relative to the reference period (right column, unit is %). Locations, where at least 80 % of models agree on the sign of change are marked with black dot.

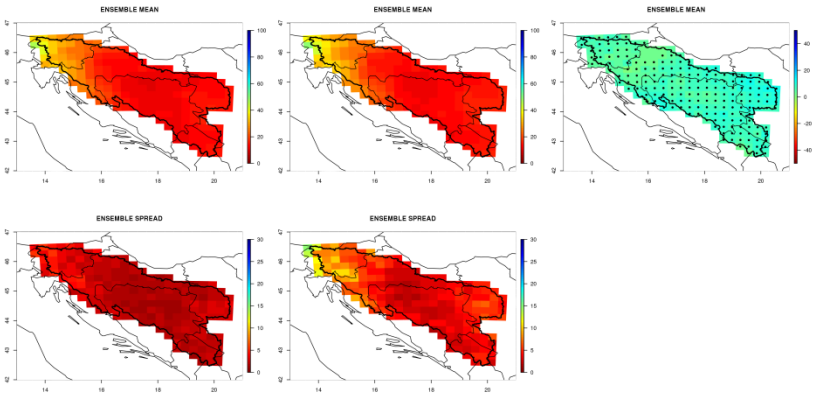

Figure 55: Projections for 95th percentile daily precipitation on wet day in spring. Shown are: ensemble mean and spread for the reference period (left column, unit is mm/day), ensemble

mean and spread for 2041-2070 (middle column, unit is mm/day) and ensemble mean of changes relative to the reference period (right column, unit is %). Locations, where at least 80 % of models agree on the sign of change are marked with black dot.

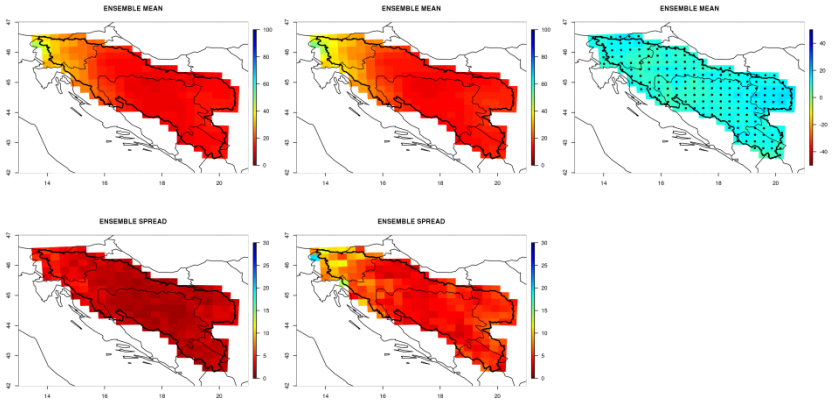

Figure 56: Projections for 95th percentile daily precipitation on wet day in spring. Shown are: ensemble mean and spread for the reference period (left column, unit is mm/day), ensemble mean and spread for 2071-2100 (middle column, unit is mm/day) and ensemble mean of changes relative to the reference period (right column, unit is %). Locations, where at least 80 % of models agree on the sign of change are marked with black dot.

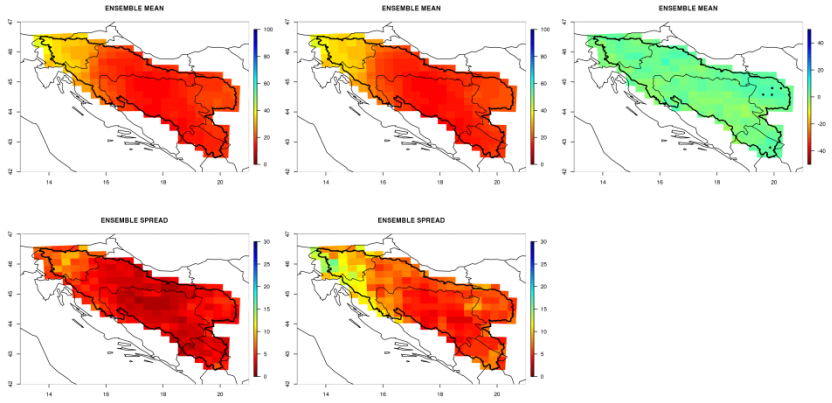

Figure 57: Projections for 95th percentile daily precipitation on wet day in summer. Shown are: ensemble mean and spread for the reference period (left column, unit is mm/day), ensemble mean and spread for 2011-2040 (middle column, unit is mm/day) and ensemble mean of changes relative to the reference period (right column, unit is %). Locations, where at least 80 % of models agree on the sign of change are marked with black dot.

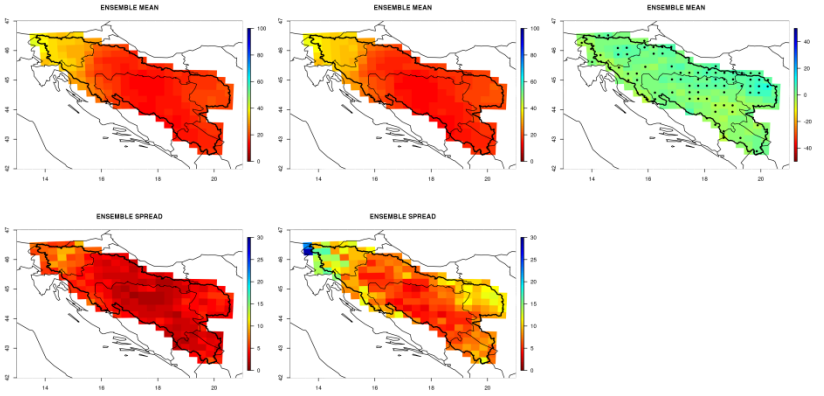

Figure 58: Projections for 95th percentile daily precipitation on wet day in summer. Shown are: ensemble mean and spread for the reference period (left column, unit is mm/day), ensemble

mean and spread for 2041-2070 (middle column, unit is mm/day) and ensemble mean of changes relative to the reference period (right column, unit is %). Locations, where at least 80 % of models agree on the sign of change are marked with black dot.

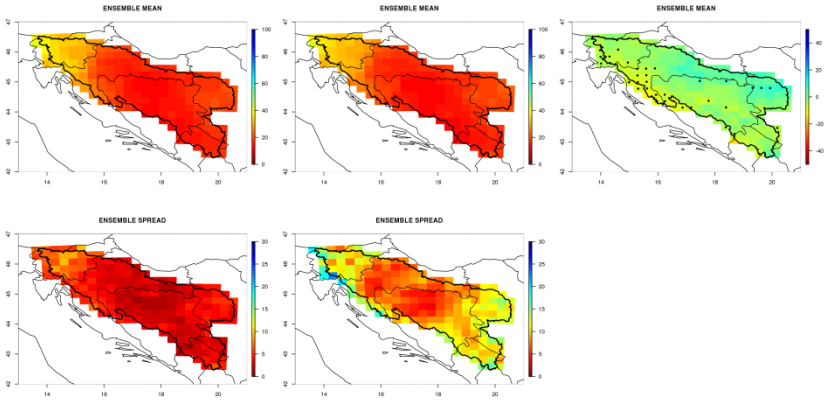

Figure 59: Projections for 95th percentile daily precipitation on wet day in summer. Shown are: ensemble mean and spread for the reference period (left column, unit is mm/day), ensemble mean and spread for 2071-2100 (middle column, unit is mm/day) and ensemble mean of changes relative to the reference period (right column, unit is %). Locations, where at least 80 % of models agree on the sign of change are marked with black dot.

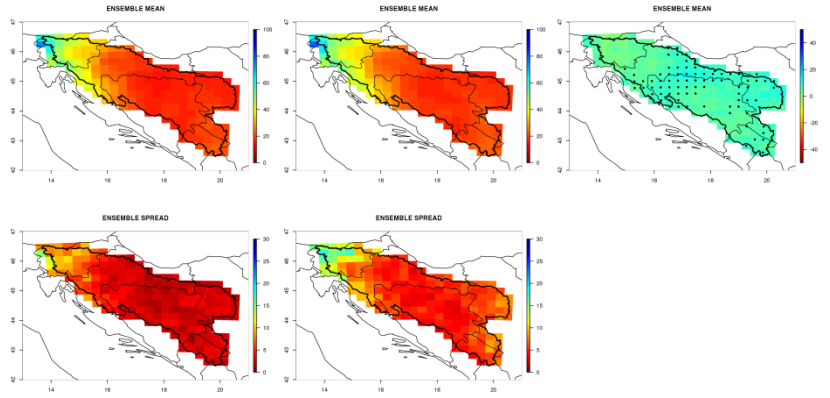

Figure 60: Projections for 95th percentile daily precipitation on wet day in autumn. Shown are: ensemble mean and spread for the reference period (left column, unit is mm/day), ensemble mean and spread for 2011-2040 (middle column, unit is mm/day) and ensemble mean of changes relative to the reference period (right column, unit is %). Locations, where at least 80 % of models agree on the sign of change are marked with black dot.

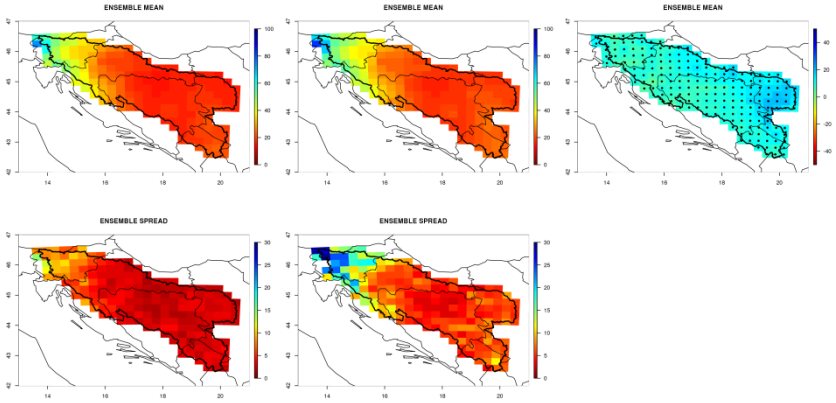

Figure 61: Projections for 95th percentile daily precipitation on wet day in autumn. Shown are: ensemble mean and spread for the reference period (left column, unit is mm/day), ensemble

mean and spread for 2041-2070 (middle column, unit is mm/day) and ensemble mean of changes relative to the reference period (right column, unit is %). Locations, where at least 80 % of models agree on the sign of change are marked with black dot.

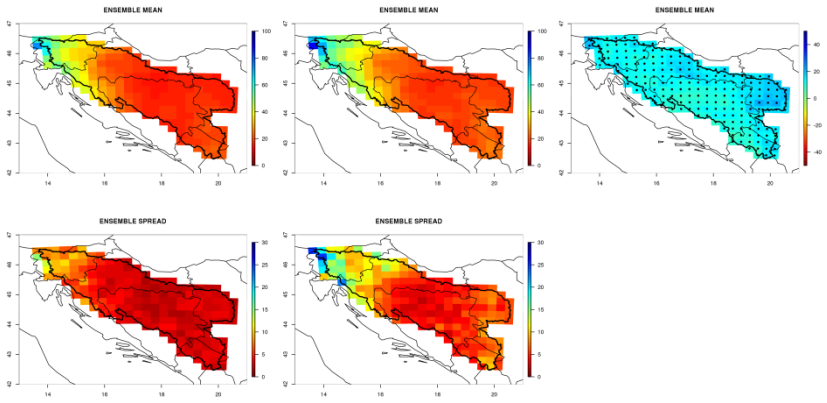

Figure 62: Projections for 95th percentile daily precipitation on wet day in autumn. Shown are: ensemble mean and spread for the reference period (left column, unit is mm/day), ensemble mean and spread for 2071-2100 (middle column, unit is mm/day) and ensemble mean of changes relative to the reference period (right column, unit is %). Locations, where at least 80 % of models agree on the sign of change are marked with black dot.

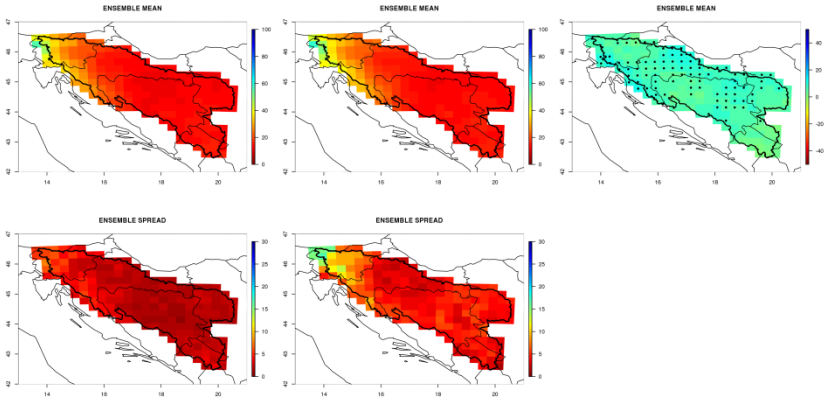

Figure 63: Projections for 95th percentile daily precipitation on wet day in winter. Shown are: ensemble mean and spread for the reference period (left column, unit is mm/day), ensemble mean and spread for 2011-2040 (middle column, unit is mm/day) and ensemble mean of changes relative to the reference period (right column, unit is %). Locations, where at least 80 % of models agree on the sign of change are marked with black dot.

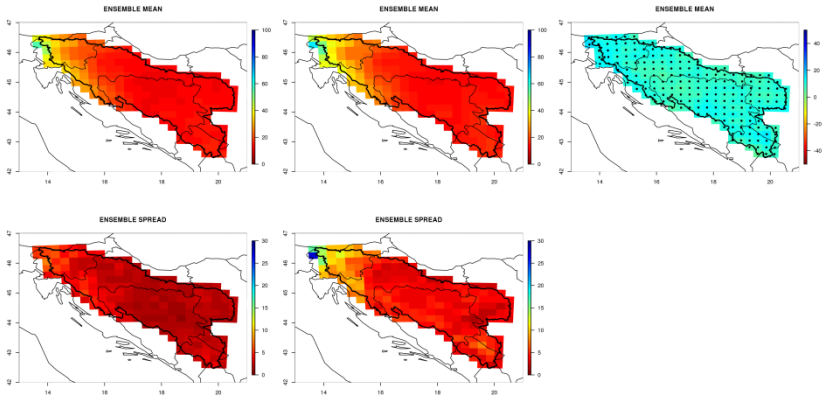

Figure 64: Projections for 95th percentile daily precipitation on wet day in winter. Shown are: ensemble mean and spread for the reference period (left column, unit is mm/day), ensemble

mean and spread for 2041-2070 (middle column, unit is mm/day) and ensemble mean of changes relative to the reference period (right column, unit is %). Locations, where at least 80 % of models agree on the sign of change are marked with black dot.

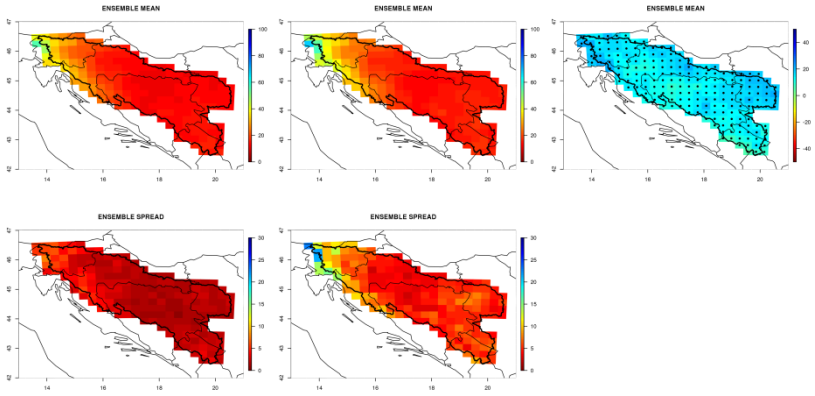

Figure 65: Projections for 95th percentile daily precipitation on wet day in winter. Shown are: ensemble mean and spread for the reference period (left column, unit is mm/day), ensemble mean and spread for 2071-2100 (middle column, unit is mm/day) and ensemble mean of changes relative to the reference period (right column, unit is %). Locations, where at least 80 % of models agree on the sign of change are marked with black dot.

Maximum 24- and 48-hour precipitation is expected to increase throughout the 21st Century (***Figures 66–89***) in spring, autumn and winter. Changes of summer maxima are spatially highly variable. In the western part of Croatia and Bosnia and Herzegovina, a decrease of up to -20 % is expected, whereas a slight increase (approximately +5 %) is expected in the north-western part of the basin. Spatial patterns of changes are similar for 24- and 48-hour maximum precipitation. The highest ensemble spread can be observed in the north-western part of the basin.

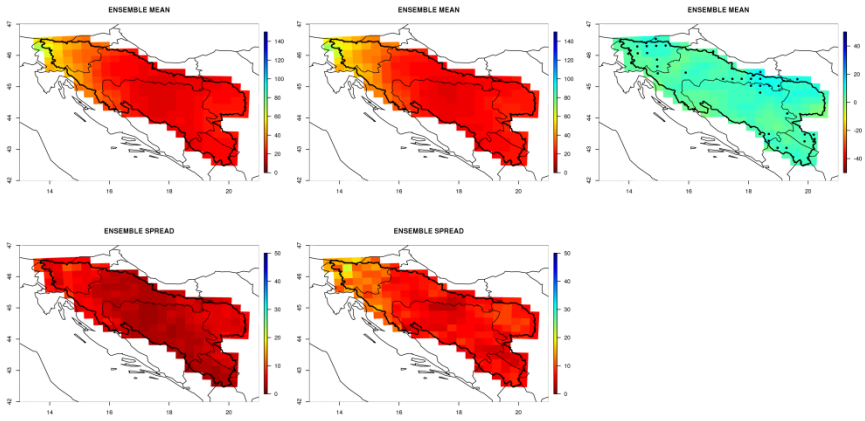

Figure 66: Projections of interannual average of maximum 24 hours precipitation on wet day in spring. Shown are: ensemble mean and spread for the reference period (left column, unit is mm/day), ensemble mean and spread for 2011-2040 (middle column, unit is mm/day) and ensemble mean of changes relative to the reference period (right column, unit is %). Locations, where at least 80 % of models agree on the sign of change are marked with black dot.

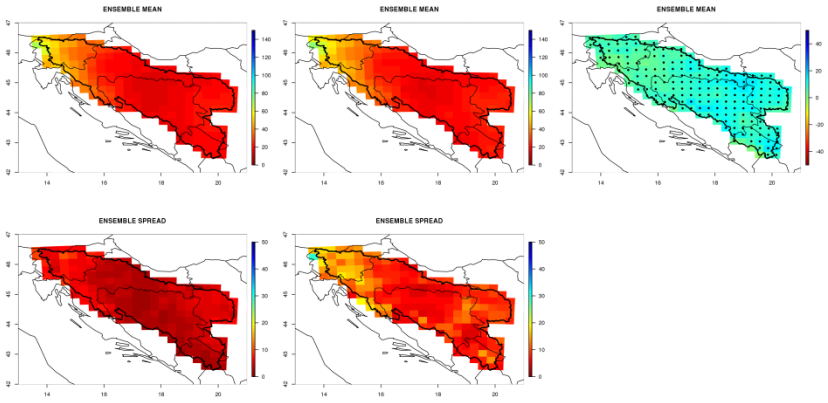

Figure 67: Projections of interannual average of maximum 24 hours precipitation on wet day in spring. Shown are: ensemble mean and spread for the reference period (left column, unit is mm/day), ensemble mean and spread for 2041-2070 (middle column, unit is mm/day) and ensemble mean of changes relative to the reference period (right column, unit is %). Locations, where at least 80 % of models agree on the sign of change are marked with black dot.

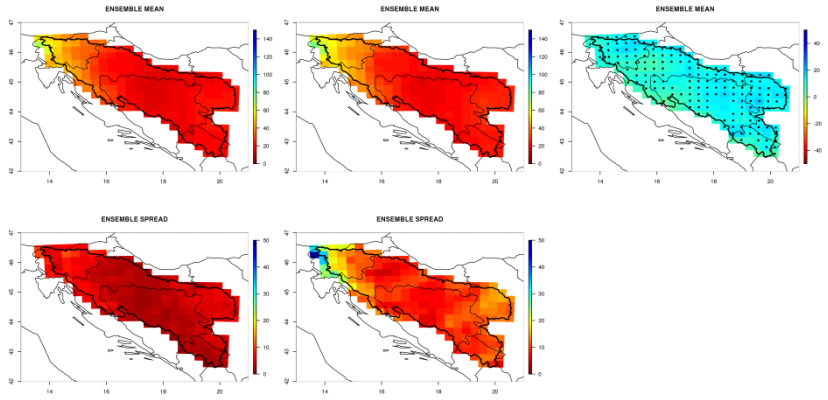

Figure 68: Projections of interannual average of maximum 24 hours precipitation on wet day in spring. Shown are: ensemble mean and spread for the reference period (left column, unit is mm/day), ensemble mean and spread for 2071-2100 (middle column, unit is mm/day) and ensemble mean of changes relative to the reference period (right column, unit is %). Locations, where at least 80 % of models agree on the sign of change are marked with black dot.

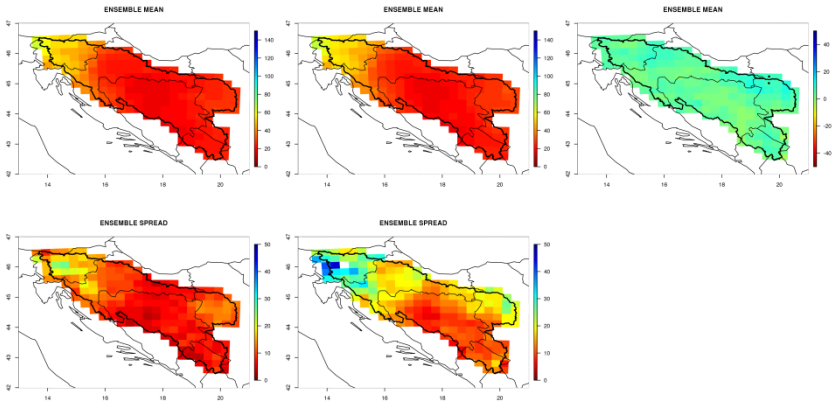

Figure 69: Projections of interannual average of maximum 24 hours precipitation on wet day in summer. Shown are: ensemble mean and spread for the reference period (left column, unit is mm/day), ensemble mean and spread for 2011-2040 (middle column, unit is mm/day) and ensemble mean of changes relative to the reference period (right column, unit is %). Locations, where at least 80 % of models agree on the sign of change are marked with black dot.

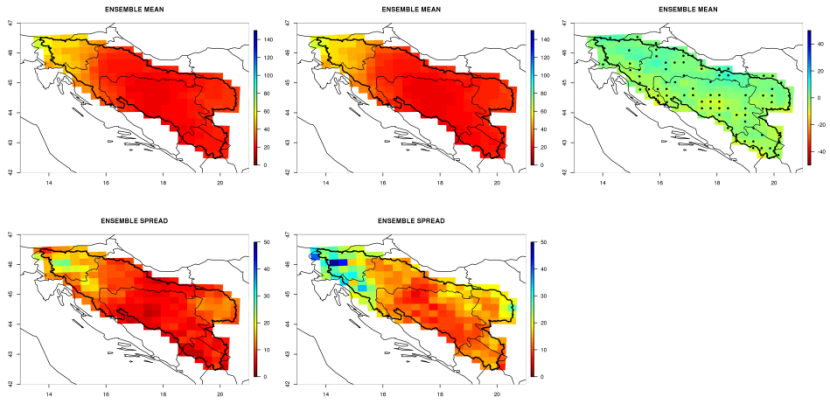

Figure 70: Projections of interannual average of maximum 24 hours precipitation on wet day in summer. Shown are: ensemble mean and spread for the reference period (left column, unit is mm/day), ensemble mean and spread for 2041-2070 (middle column, unit is mm/day) and ensemble mean of changes relative to the reference period (right column, unit is %). Locations, where at least 80 % of models agree on the sign of change are marked with black dot.

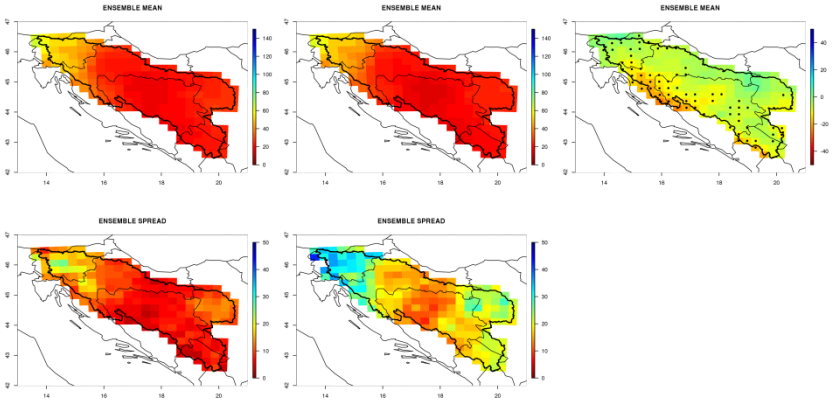

Figure 71: Projections of interannual average of maximum 24 hours precipitation on wet day in summer. Shown are: ensemble mean and spread for the reference period (left column, unit is mm/day), ensemble mean and spread for 2071-2100 (middle column, unit is mm/day) and ensemble mean of changes relative to the reference period (right column, unit is %). Locations, where at least 80 % of models agree on the sign of change are marked with black dot.

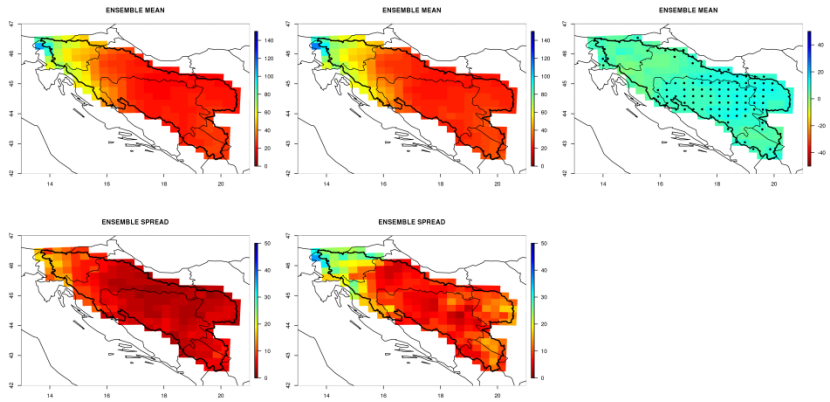

Figure 72: Projections of interannual average of maximum 24 hours precipitation on wet day in autumn. Shown are: ensemble mean and spread for the reference period (left column, unit is mm/day), ensemble mean and spread for 2011-2040 (middle column, unit is mm/day) and ensemble mean of changes relative to the reference period (right column, unit is %). Locations, where at least 80 % of models agree on the sign of change are marked with black dot.

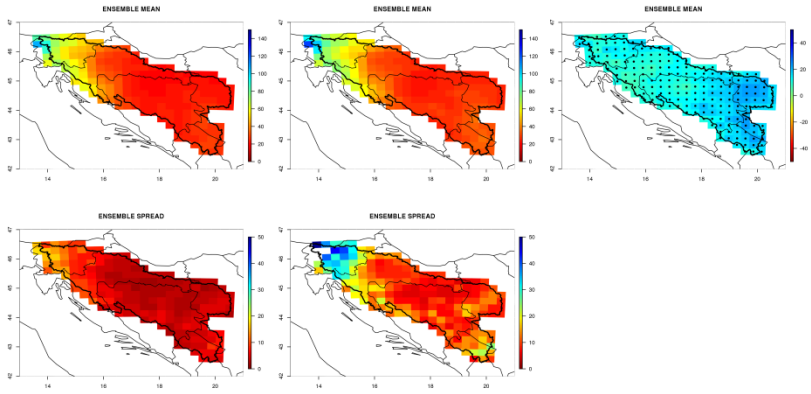

Figure 73: Projections of interannual average of maximum 24 hours precipitation on wet day in autumn. Shown are: ensemble mean and spread for the reference period (left column, unit is mm/day), ensemble mean and spread for 2041-2070 (middle column, unit is mm/day) and ensemble mean of changes relative to the reference period (right column, unit is %). Locations, where at least 80 % of models agree on the sign of change are marked with black dot.

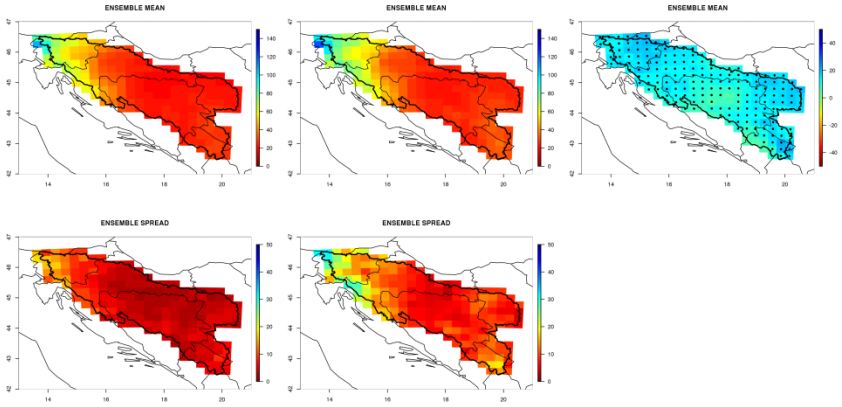

Figure 74: Projections of interannual average of maximum 24 hours precipitation on wet day in autumn. Shown are: ensemble mean and spread for the reference period (left column, unit is mm/day), ensemble mean and spread for 2071-2100 (middle column, unit is mm/day) and ensemble mean of changes relative to the reference period (right column, unit is %). Locations, where at least 80 % of models agree on the sign of change are marked with black dot.

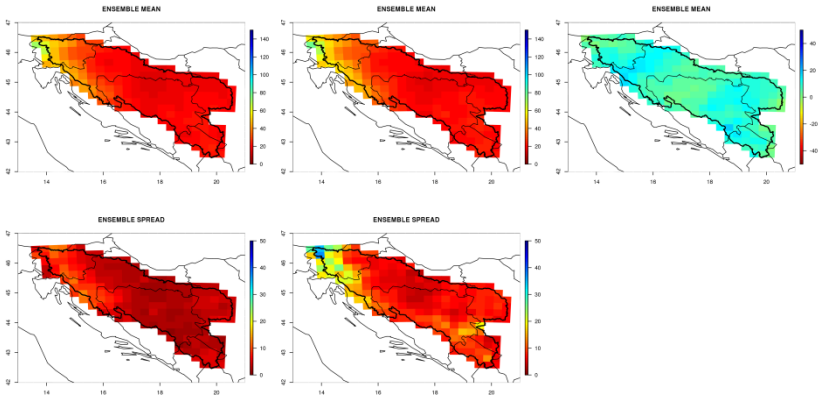

Figure 75: Projections of interannual average of maximum 24 hours precipitation on wet day in winter. Shown are: ensemble mean and spread for the reference period (left column, unit is mm/day), ensemble mean and spread for 2011-2040 (middle column, unit is mm/day) and ensemble mean of changes relative to the reference period (right column, unit is %). Locations, where at least 80 % of models agree on the sign of change are marked with black dot.

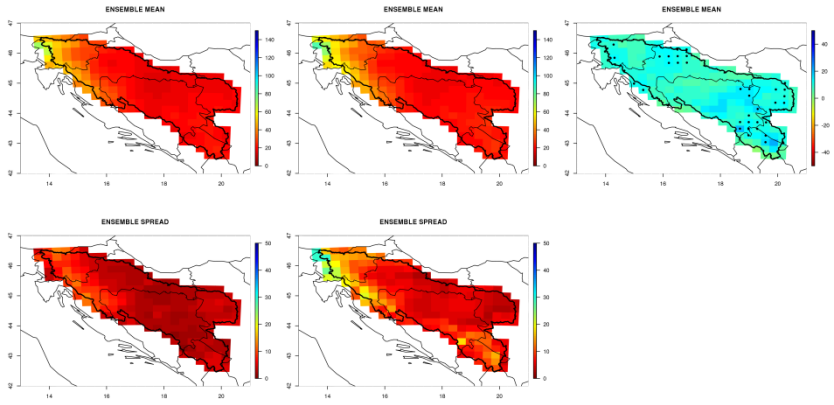

Figure 76: Projections of interannual average of maximum 24 hours precipitation on wet day in winter. Shown are: ensemble mean and spread for the reference period (left column, unit is mm/day), ensemble mean and spread for 2041-2070 (middle column, unit is mm/day) and ensemble mean of changes relative to the reference period (right column, unit is %). Locations, where at least 80 % of models agree on the sign of change are marked with black dot.

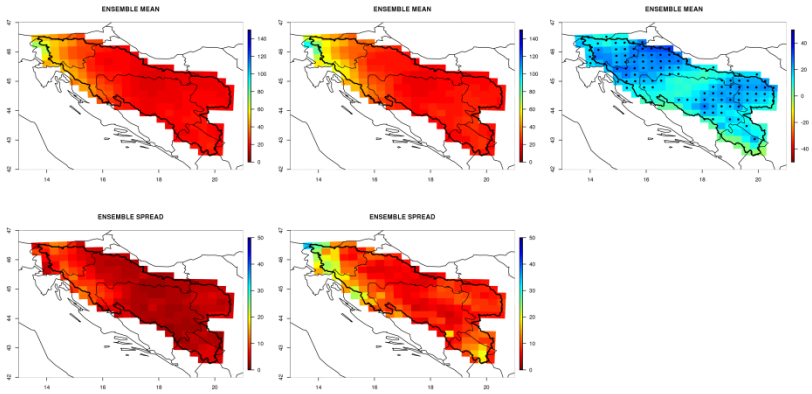

Figure 77: Projections of interannual average of maximum 24 hours precipitation on wet day in winter. Shown are: ensemble mean and spread for the reference period (left column, unit is mm/day), ensemble mean and spread for 2071-2100 (middle column, unit is mm/day) and ensemble mean of changes relative to the reference period (right column, unit is %). Locations, where at least 80 % of models agree on the sign of change are marked with black dot.

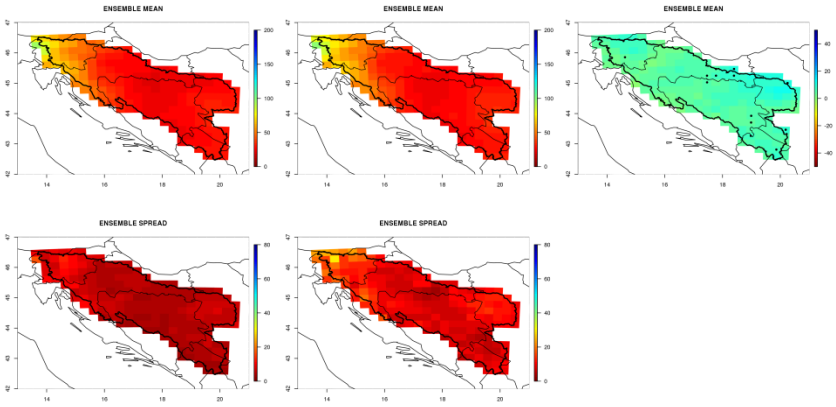

Figure 78: Projections of interannual average of maximum 48 hours precipitation on wet day in spring. Shown are: ensemble mean and spread for the reference period (left column, unit is mm/day), ensemble mean and spread for 2011-2040 (middle column, unit is mm/day) and ensemble mean of changes relative to the reference period (right column, unit is %). Locations, where at least 80 % of models agree on the sign of change are marked with black dot.

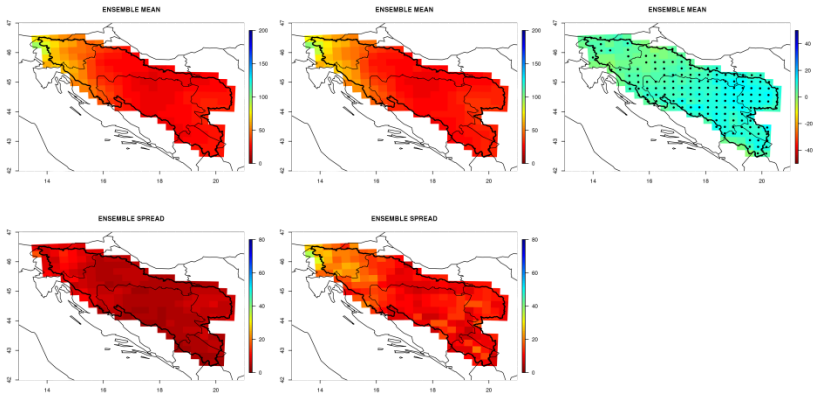

Figure 79: Projections of interannual average of maximum 48 hours precipitation on wet day in spring. Shown are: ensemble mean and spread for the reference period (left column, unit is mm/day), ensemble mean and spread for 2041-2070 (middle column, unit is mm/day) and ensemble mean of changes relative to the reference period (right column, unit is %). Locations, where at least 80 % of models agree on the sign of change are marked with black dot.

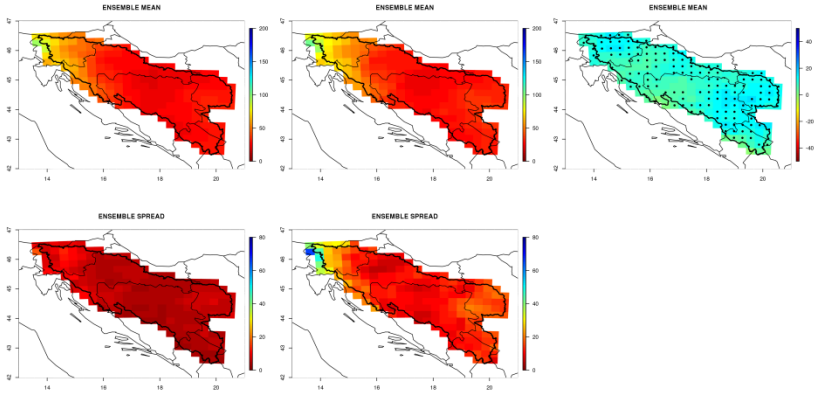

Figure 80: Projections of interannual average of maximum 48 hours precipitation on wet day in spring. Shown are: ensemble mean and spread for the reference period (left column, unit is mm/day), ensemble mean and spread for 2071-2100 (middle column, unit is mm/day) and ensemble mean of changes relative to the reference period (right column, unit is %). Locations, where at least 80 % of models agree on the sign of change are marked with black dot.

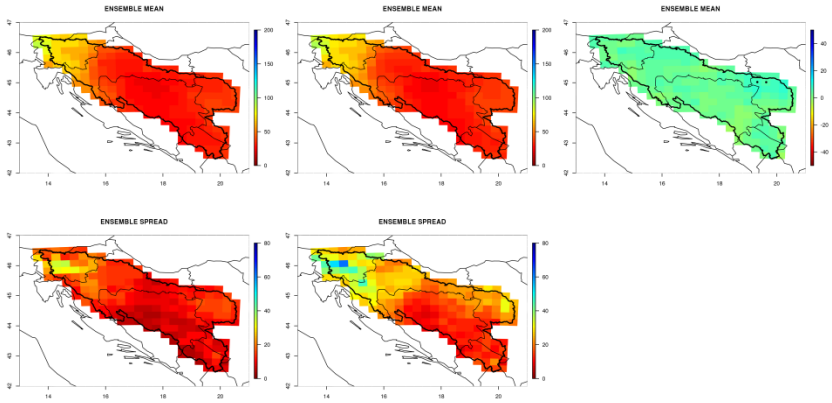

Figure 81: Projections of interannual average of maximum 48 hours precipitation on wet day in summer. Shown are: ensemble mean and spread for the reference period (left column, unit is mm/day), ensemble mean and spread for 2011-2040 (middle column, unit is mm/day) and ensemble mean of changes relative to the reference period (right column, unit is %). Locations, where at least 80 % of models agree on the sign of change are marked with black dot.

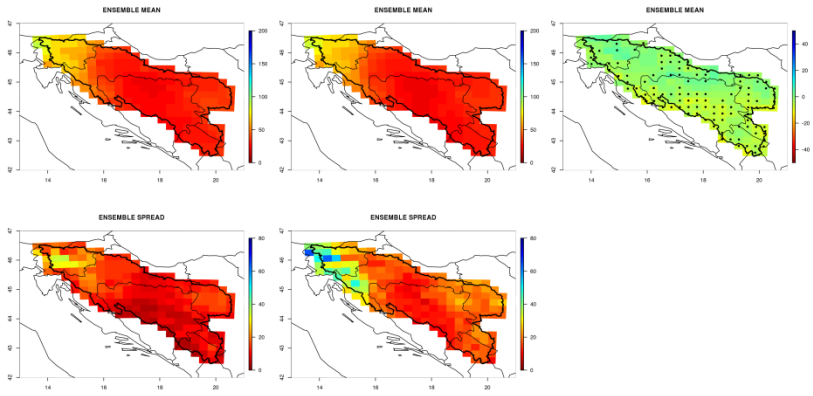

Figure 82: Projections of interannual average of maximum 48 hours precipitation on wet day in summer. Shown are: ensemble mean and spread for the reference period (left column, unit is mm/day), ensemble mean and spread for 2041-2070 (middle column, unit is mm/day) and ensemble mean of changes relative to the reference period (right column, unit is %). Locations, where at least 80 % of models agree on the sign of change are marked with black dot.

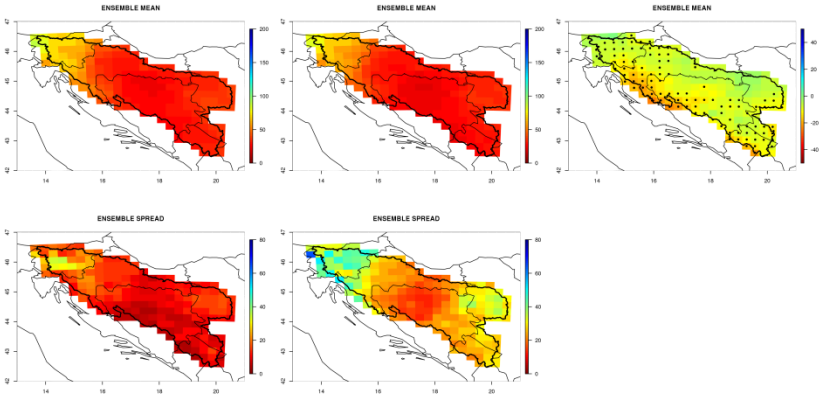

Figure 83: Projections of interannual average of maximum 48 hours precipitation on wet day in summer. Shown are: ensemble mean and spread for the reference period (left column, unit is mm/day), ensemble mean and spread for 2071-2100 (middle column, unit is mm/day) and ensemble mean of changes relative to the reference period (right column, unit is %). Locations, where at least 80 % of models agree on the sign of change are marked with black dot.

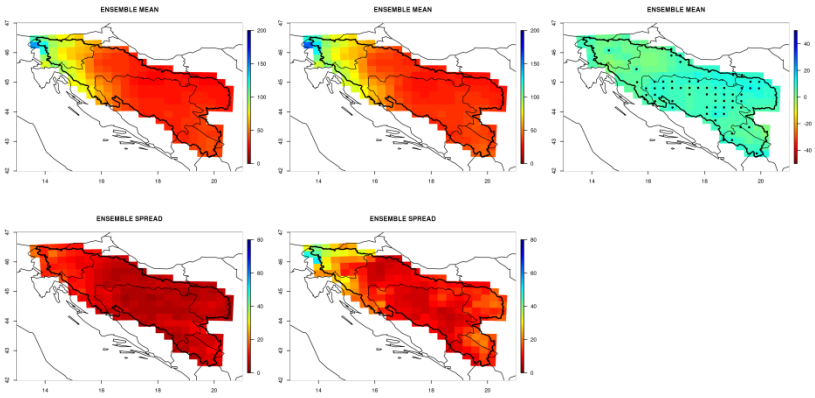

Figure 84: Projections of interannual average of maximum 48 hours precipitation on wet day in autumn. Shown are: ensemble mean and spread for the reference period (left column, unit is mm/day), ensemble mean and spread for 2011-2040 (middle column, unit is mm/day) and ensemble mean of changes relative to the reference period (right column, unit is %). Locations, where at least 80 % of models agree on the sign of change are marked with black dot.

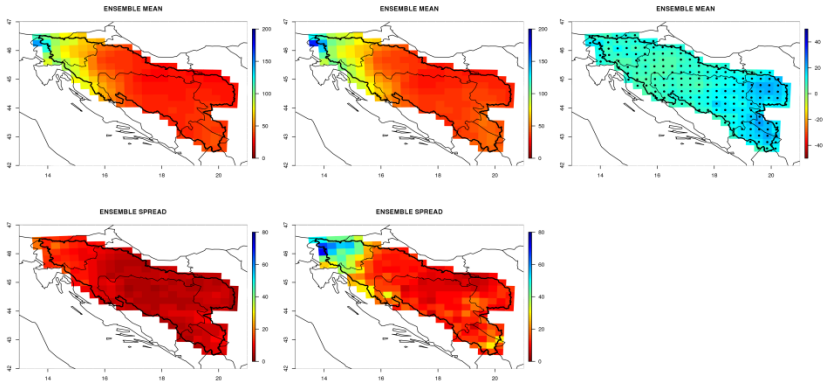

Figure 85: Projections of interannual average of maximum 48 hours precipitation on wet day in autumn. Shown are: ensemble mean and spread for the reference period (left column, unit is mm/day), ensemble mean and spread for 2041-2070 (middle column, unit is mm/day) and ensemble mean of changes relative to the reference period (right column, unit is %). Locations, where at least 80 % of models agree on the sign of change are marked with black dot.

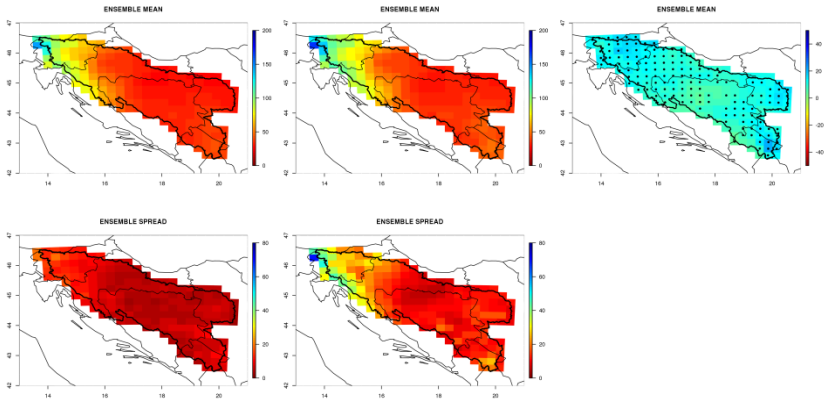

Figure 86: Projections of interannual average of maximum 48 hours precipitation on wet day in autumn. Shown are: ensemble mean and spread for the reference period (left column, unit is mm/day), ensemble mean and spread for 2071-2100 (middle column, unit is mm/day) and ensemble mean of changes relative to the reference period (right column, unit is %). Locations, where at least 80 % of models agree on the sign of change are marked with black dot.

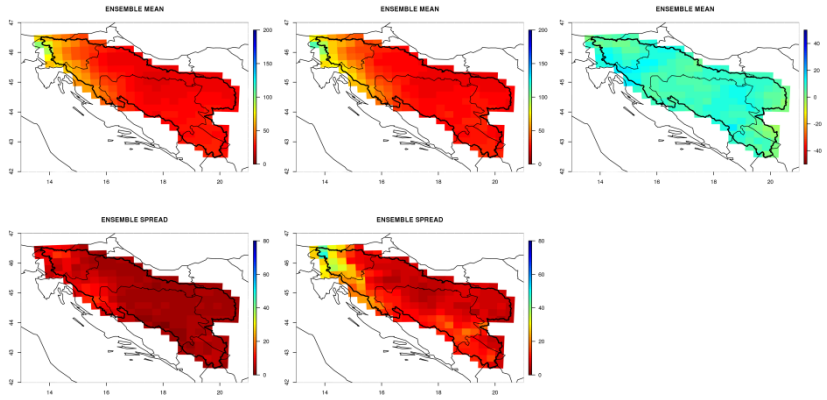

Figure 87: Projections of interannual average of maximum 48 hours precipitation on wet day in winter. Shown are: ensemble mean and spread for the reference period (left column, unit is mm/day), ensemble mean and spread for 2011-2040 (middle column, unit is mm/day) and ensemble mean of changes relative to the reference period (right column, unit is %). Locations, where at least 80 % of models agree on the sign of change are marked with black dot.

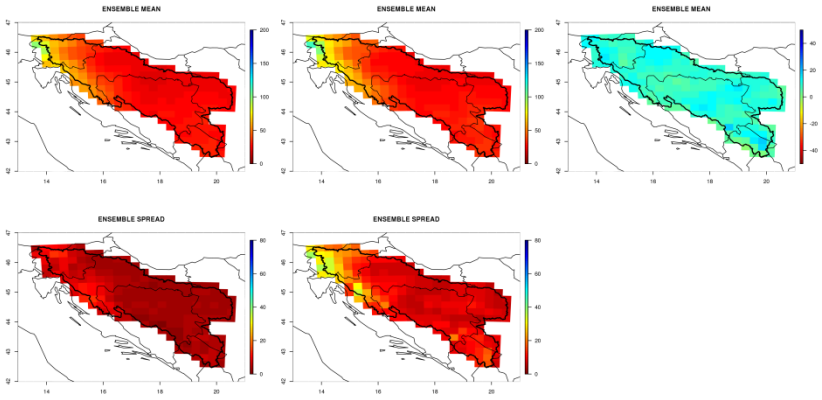

Figure 88: Projections of interannual average of maximum 48 hours precipitation on wet day in winter. Shown are: ensemble mean and spread for the reference period (left column, unit is mm/day), ensemble mean and spread for 2041-2070 (middle column, unit is mm/day) and ensemble mean of changes relative to the reference period (right column, unit is %). Locations, where at least 80 % of models agree on the sign of change are marked with black dot.

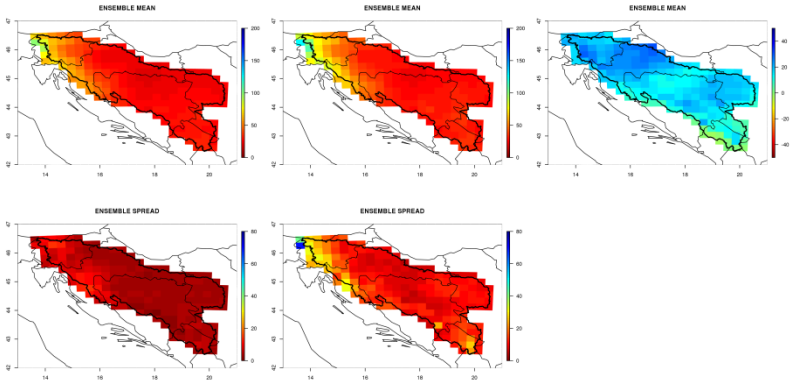

Figure 89: Projections of interannual average of maximum 48 hours precipitation on wet day in winter. Shown are: ensemble mean and spread for the reference period (left column, unit is mm/day), ensemble mean and spread for 2071-2100 (middle column, unit is mm/day) and ensemble mean of changes relative to the reference period (right column, unit is %). Locations, where at least 80 % of models agree on the sign of change are marked with black dot.

Figures 90–113 show changes in precipitation intensities with return periods of 20 and 100 years. Precipitation intensities with 20- and 100-year return periods are expected to increase in spring in the central part of the basin. The change signal is, however, weak in other parts of the basin, especially for the 100-year return period. In summer, precipitation intensity with a return period of 100 years is expected to increase in parts of the eastern basin; the model spread tends to be quite high, weakening the reliability of the projections. The ensemble signal for summer is stronger for the 20-year return period, when an increase can be observed in the southeastern part of the basin. In autumn, a general increase of the 20-year and 100-year return levels can be observed over the majority of the basin territory. The highest increase of return levels can be observed in the southern part of the basin. Higher regional differences prevail in the case of winter return levels, when an increase is expected in Croatia and parts of Bosnia and Herzegovina.

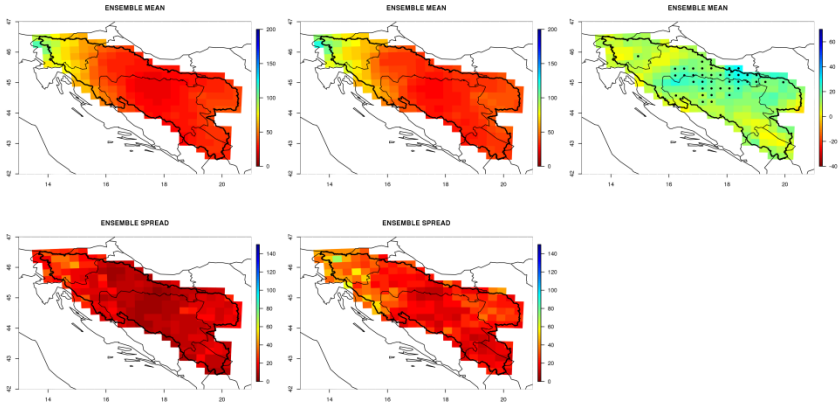

Figure 90: Projections of precipitation intensity on wet day in spring with return period 20 years. Shown are: ensemble mean and spread for the reference period (left column, unit is mm/day), ensemble mean and spread for 2011-2040 (middle column, unit is mm/day) and ensemble mean of changes relative to the reference period (right column, unit is %). Locations, where at least 80 % of models agree on the sign of change are marked with black dot.

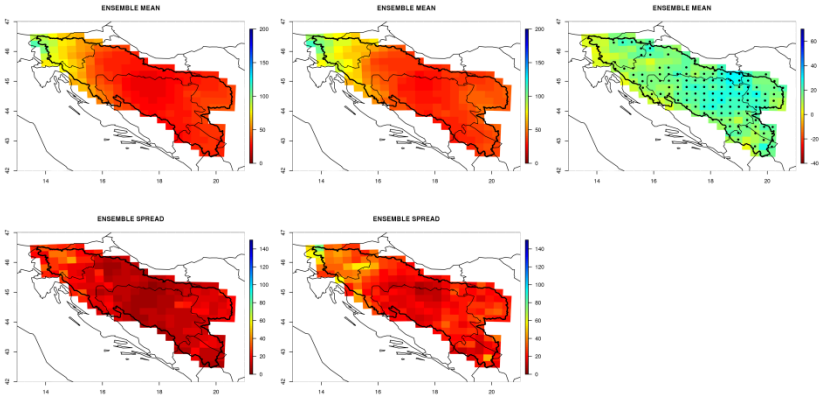

Figure 91: Projections of precipitation intensity on wet day in spring with return period 20 years. Shown are: ensemble mean and spread for the reference period (left column, unit is mm/day), ensemble mean and spread for 2041-2070 (middle column, unit is mm/day) and ensemble mean of changes relative to the reference period (right column, unit is %). Locations, where at least 80 % of models agree on the sign of change are marked with black dot.

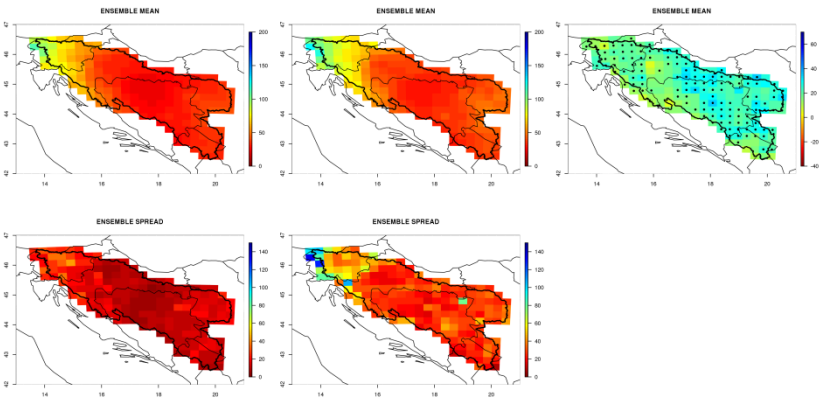

Figure 92: Projections of precipitation intensity on wet day in spring with return period 20 years. Shown are: ensemble mean and spread for the reference period (left column, unit is mm/day), ensemble mean and spread for 2071-2100 (middle column, unit is mm/day) and ensemble mean of changes relative to the reference period (right column, unit is %). Locations, where at least 80 % of models agree on the sign of change are marked with black dot.

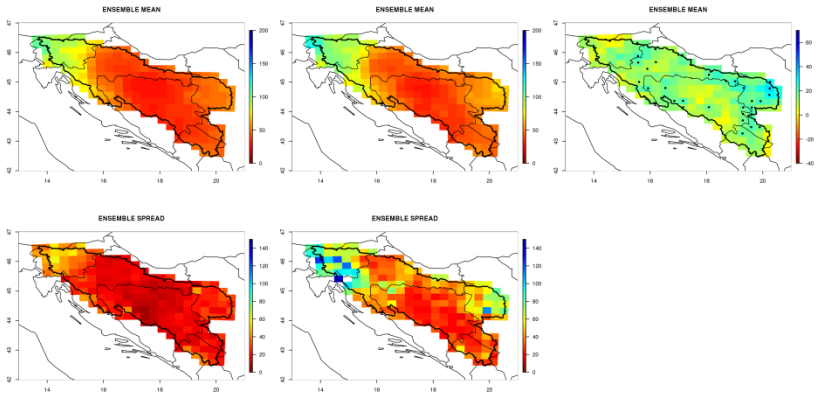

Figure 93: Projections of precipitation intensity on wet day in summer with return period 20 years. Shown are: ensemble mean and spread for the reference period (left column, unit is mm/day), ensemble mean and spread for 2011-2040 (middle column, unit is mm/day) and ensemble mean of changes relative to the reference period (right column, unit is %). Locations, where at least 80 % of models agree on the sign of change are marked with black dot.

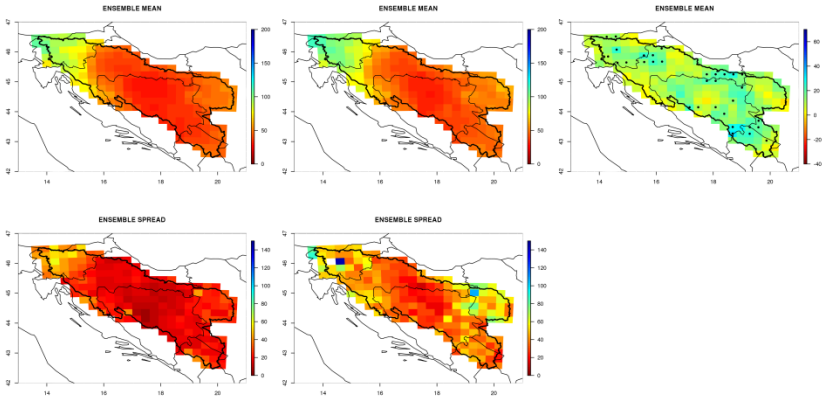

Figure 94: Projections of precipitation intensity on wet day in summer with return period 20 years. Shown are: ensemble mean and spread for the reference period (left column, unit is mm/day), ensemble mean and spread for 2041-2070 (middle column, unit is mm/day) and ensemble mean of changes relative to the reference period (right column, unit is %). Locations, where at least 80 % of models agree on the sign of change are marked with black dot.

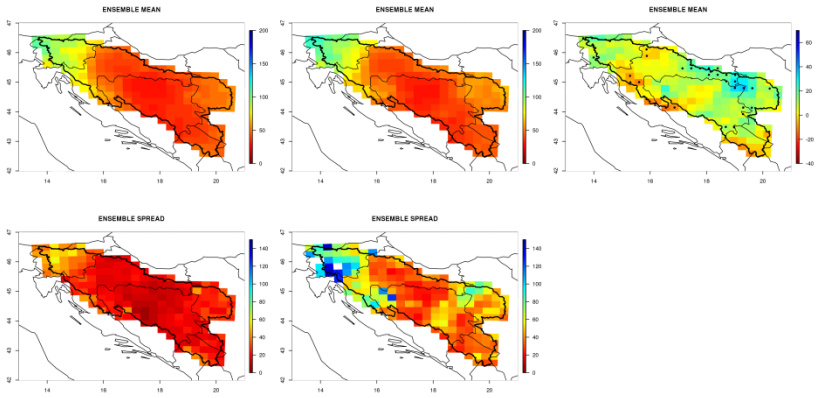

Figure 95: Projections of precipitation intensity on wet day in summer with return period 20 years. Shown are: ensemble mean and spread for the reference period (left column, unit is mm/day), ensemble mean and spread for 2071-2100 (middle column, unit is mm/day) and ensemble mean of changes relative to the reference period (right column, unit is %). Locations, where at least 80 % of models agree on the sign of change are marked with black dot.

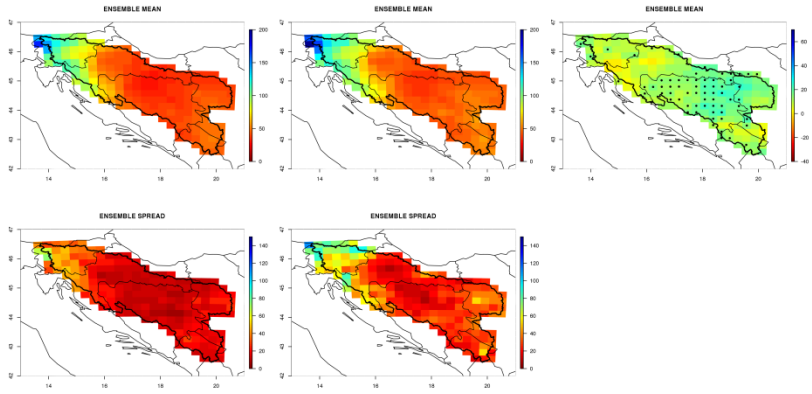

Figure 96: Projections of precipitation intensity on wet day in autumn with return period 20 years. Shown are: ensemble mean and spread for the reference period (left column, unit is mm/day), ensemble mean and spread for 2011-2040 (middle column, unit is mm/day) and ensemble mean of changes relative to the reference period (right column, unit is %). Locations, where at least 80 % of models agree on the sign of change are marked with black dot.

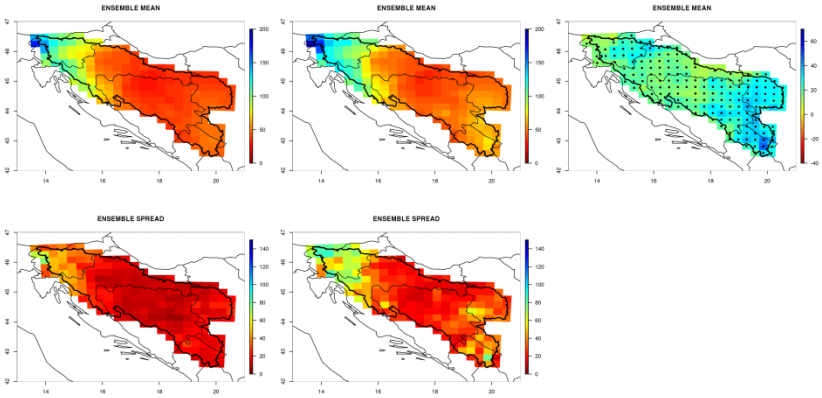

Figure 97: Projections of precipitation intensity on wet day in autumn with return period 20 years. Shown are: ensemble mean and spread for the reference period (left column, unit is mm/day), ensemble mean and spread for 2041-2070 (middle column, unit is mm/day) and ensemble mean of changes relative to the reference period (right column, unit is %). Locations, where at least 80 % of models agree on the sign of change are marked with black dot.

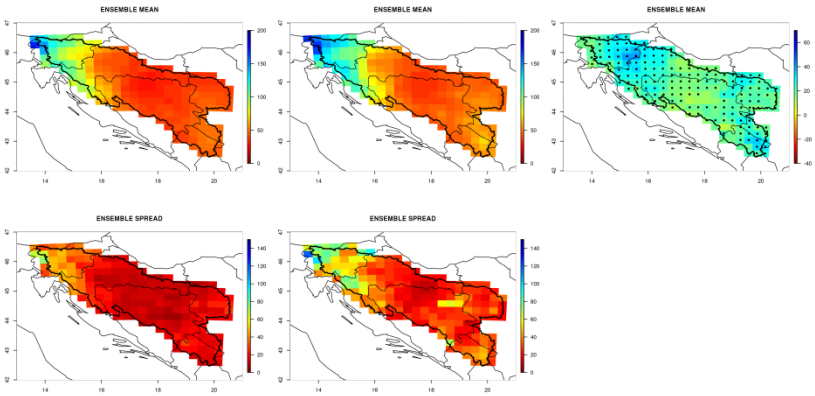

Figure 98: Projections of precipitation intensity on wet day in autumn with return period 20 years. Shown are: ensemble mean and spread for the reference period (left column, unit is mm/day), ensemble mean and spread for 2071-2100 (middle column, unit is mm/day) and ensemble mean of changes relative to the reference period (right column, unit is %). Locations, where at least 80 % of models agree on the sign of change are marked with black dot.

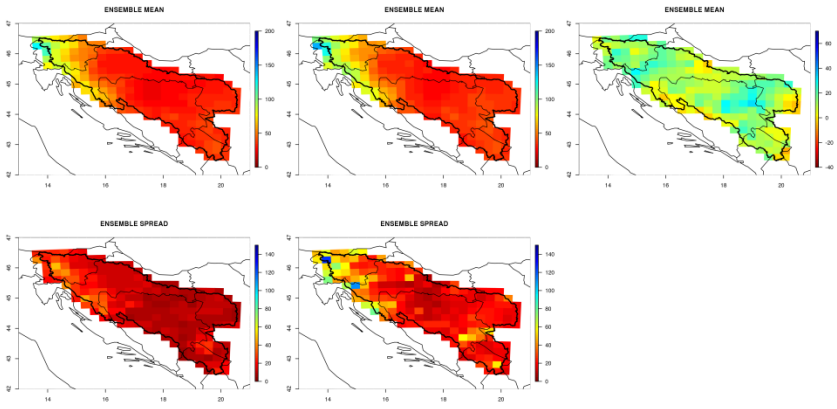

Figure 99: Projections of precipitation intensity on wet day in winter with return period 20 years. Shown are: ensemble mean and spread for the reference period (left column, unit is mm/day), ensemble mean and spread for 2011-2040 (middle column, unit is mm/day) and ensemble mean of changes relative to the reference period (right column, unit is %). Locations, where at least 80 % of models agree on the sign of change are marked with black dot.

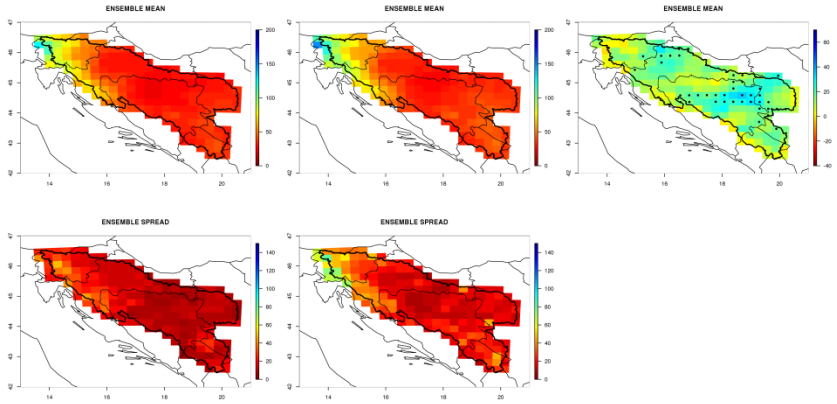

Figure 100: Projections of precipitation intensity on wet day in winter with return period 20 years. Shown are: ensemble mean and spread for the reference period (left column, unit is mm/day), ensemble mean and spread for 2041-2070 (middle column, unit is mm/day) and ensemble mean of changes relative to the reference period (right column, unit is %). Locations, where at least 80 % of models agree on the sign of change are marked with black dot.

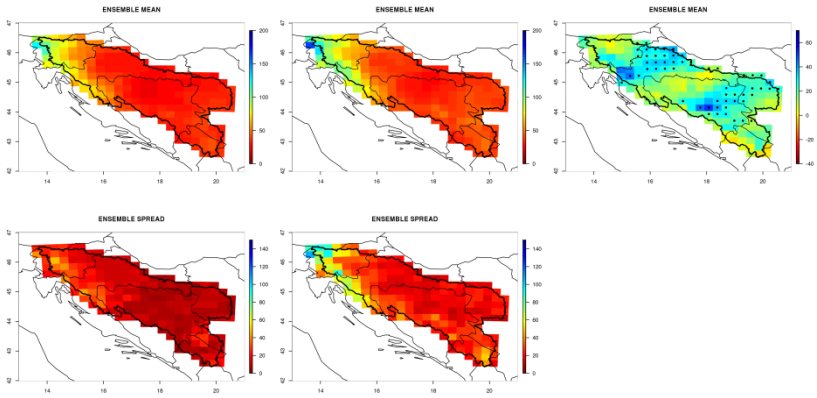

Figure 101: Projections of precipitation intensity on wet day in winter with return period 20 years. Shown are: ensemble mean and spread for the reference period (left column, unit is mm/day), ensemble mean and spread for 2071-2100 (middle column, unit is mm/day) and ensemble mean of changes relative to the reference period (right column, unit is %). Locations, where at least 80 % of models agree on the sign of change are marked with black dot.

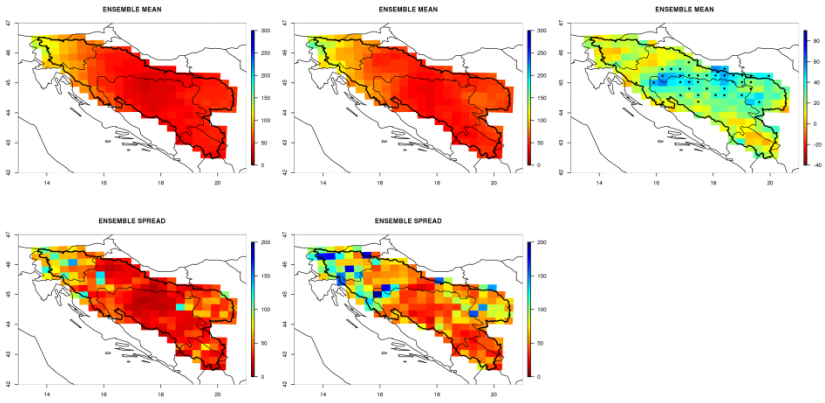

Figure 102: Projections of precipitation intensity on wet day in spring with return period 100 years. Shown are: ensemble mean and spread for the reference period (left column, unit is mm/day), ensemble mean and spread for 2011-2040 (middle column, unit is mm/day) and ensemble mean of changes relative to the reference period (right column, unit is %). Locations, where at least 80 % of models agree on the sign of change are marked with black dot.

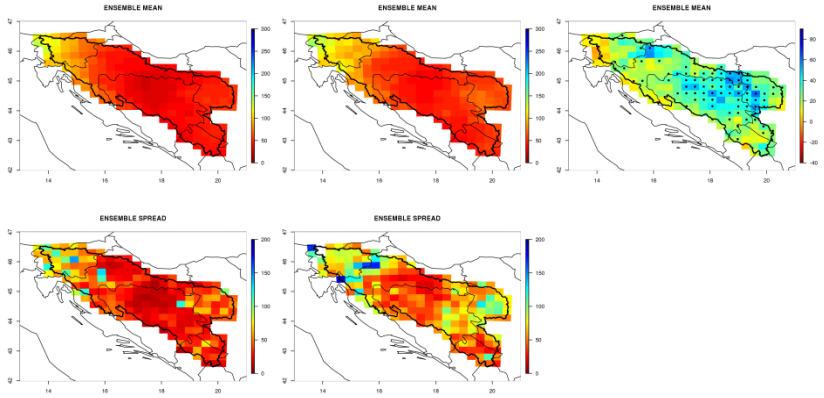

Figure 103: Projections of precipitation intensity on wet day in spring with return period 100 years. Shown are: ensemble mean and spread for the reference period (left column, unit is mm/day), ensemble mean and spread for 2041-2070 (middle column, unit is mm/day) and ensemble mean of changes relative to the reference period (right column, unit is %). Locations, where at least 80 % of models agree on the sign of change are marked with black dot.

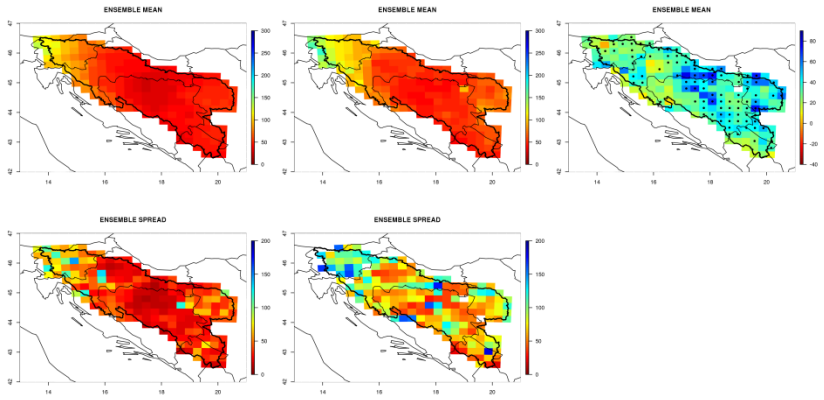

Figure 104: Projections of precipitation intensity on wet day in spring with return period 100 years. Shown are: ensemble mean and spread for the reference period (left column, unit is mm/day), ensemble mean and spread for 2071-2100 (middle column, unit is mm/day) and ensemble mean of changes relative to the reference period (right column, unit is %). Locations, where at least 80 % of models agree on the sign of change are marked with black dot.

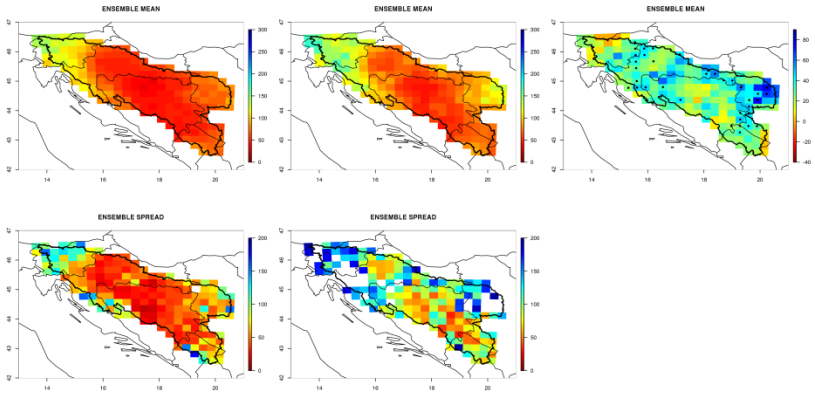

Figure 105: Projections of precipitation intensity on wet day in summer with return period 100 years. Shown are: ensemble mean and spread for the reference period (left column, unit is mm/day), ensemble mean and spread for 2011-2040 (middle column, unit is mm/day) and ensemble mean of changes relative to the reference period (right column, unit is %). Locations, where at least 80 % of models agree on the sign of change are marked with black dot.

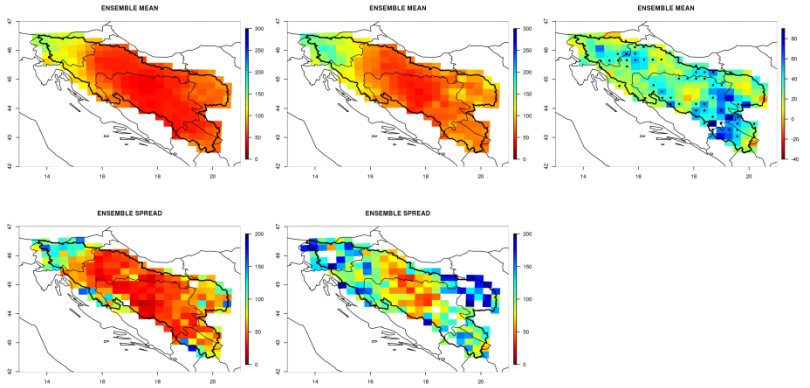

Figure 106: Projections of precipitation intensity on wet day in summer with return period 100 years. Shown are: ensemble mean and spread for the reference period (left column, unit is mm/day), ensemble mean and spread for 2041-2070 (middle column, unit is mm/day) and ensemble mean of changes relative to the reference period (right column, unit is %). Locations, where at least 80 % of models agree on the sign of change are marked with black dot.

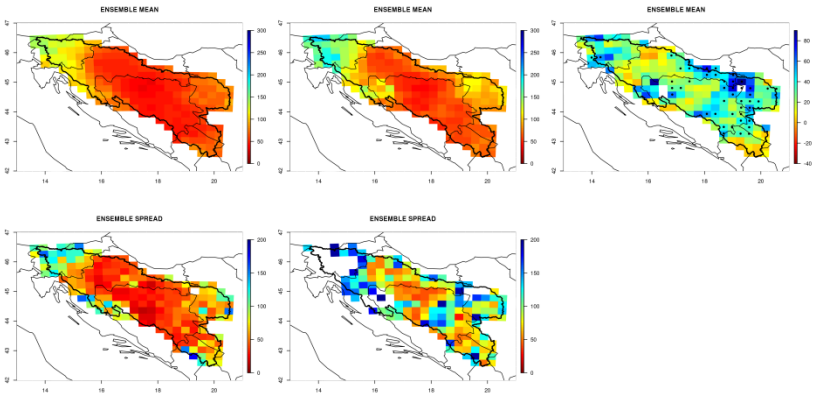

Figure 107: Projections of precipitation intensity on wet day in summer with return period 100 years. Shown are: ensemble mean and spread for the reference period (left column, unit is mm/day), ensemble mean and spread for 2071-2100 (middle column, unit is mm/day) and ensemble mean of changes relative to the reference period (right column, unit is %). Locations, where at least 80 % of models agree on the sign of change are marked with black dot.

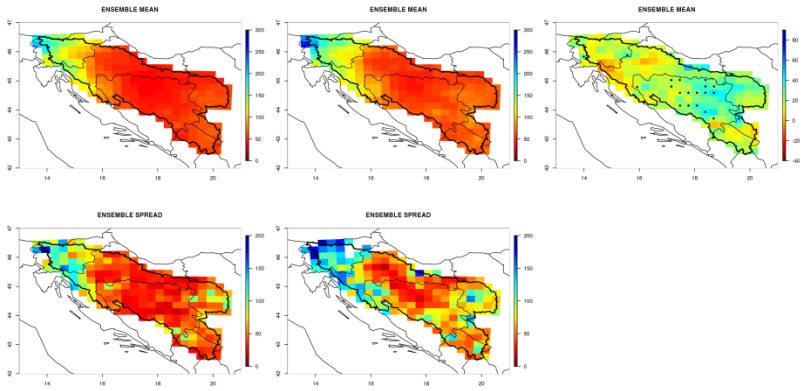

Figure 108: Projections of precipitation intensity on wet day in autumn with return period 100 years. Shown are: ensemble mean and spread for the reference period (left column, unit is mm/day), ensemble mean and spread for 2011-2040 (middle column, unit is mm/day) and ensemble mean of changes relative to the reference period (right column, unit is %). Locations, where at least 80 % of models agree on the sign of change are marked with black dot.

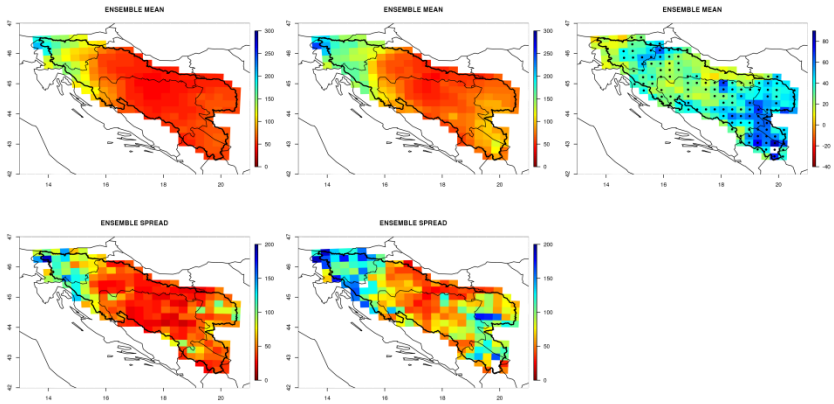

Figure 109: Projections of precipitation intensity on wet day in autumn with return period 100 years. Shown are: ensemble mean and spread for the reference period (left column, unit is mm/day), ensemble mean and spread for 2041-2070 (middle column, unit is mm/day) and ensemble mean of changes relative to the reference period (right column, unit is %). Locations, where at least 80 % of models agree on the sign of change are marked with black dot.

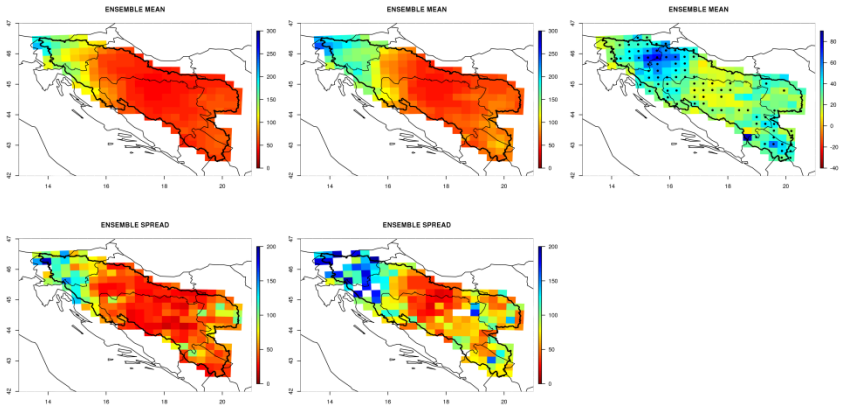

Figure 110: Projections of precipitation intensity on wet day in autumn with return period 100 years. Shown are: ensemble mean and spread for the reference period (left column, unit is mm/day), ensemble mean and spread for 2071-2100 (middle column, unit is mm/day) and ensemble mean of changes relative to the reference period (right column, unit is %). Locations, where at least 80 % of models agree on the sign of change are marked with black dot.

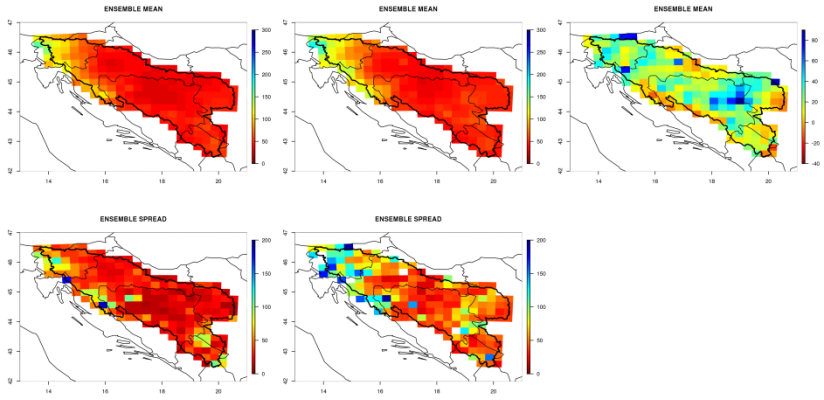

Figure 111: Projections of precipitation intensity on wet day in winter with return period 100 years. Shown are: ensemble mean and spread for the reference period (left column, unit is mm/day), ensemble mean and spread for 2011-2040 (middle column, unit is mm/day) and ensemble mean of changes relative to the reference period (right column, unit is %). Locations, where at least 80 % of models agree on the sign of change are marked with black dot.

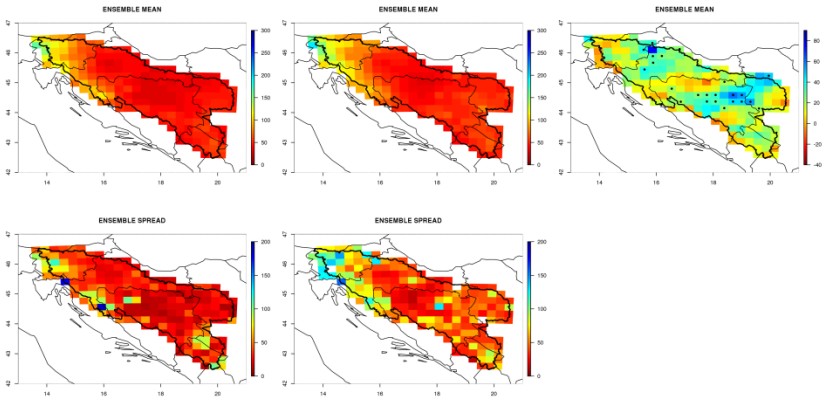

Figure 112: Projections of precipitation intensity on wet day in winter with return period 100 years. Shown are: ensemble mean and spread for the reference period (left column, unit is mm/day), ensemble mean and spread for 2041-2070 (middle column, unit is mm/day) and ensemble mean of changes relative to the reference period (right column, unit is %). Locations, where at least 80 % of models agree on the sign of change are marked with black dot.

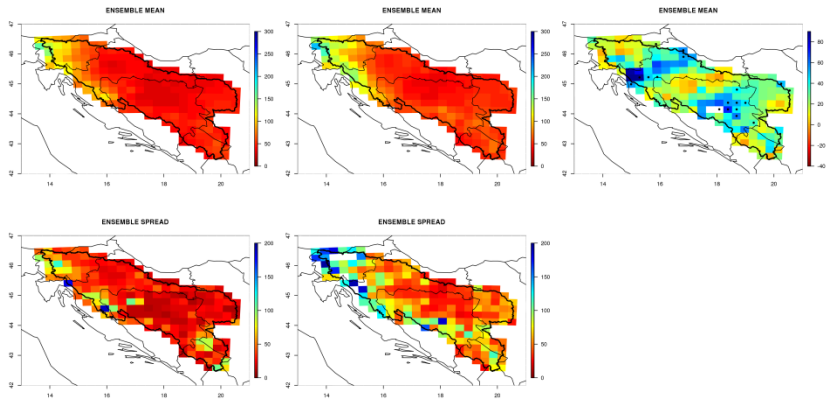

Figure 113: Projections of precipitation intensity on wet day in winter with return period 100 years. Shown are: ensemble mean and spread for the reference period (left column, unit is mm/day), ensemble mean and spread for 2071-2100 (middle column, unit is mm/day) and ensemble mean of changes relative to the reference period (right column, unit is %). Locations, where at least 80 % of models agree on the sign of change are marked with black dot.

4.3.3 TEMPERATURE PROJECTIONS

Figures 114–125 represent seasonal temperature projections for three periods in the 21st Century. All models in the ensemble agree in the sign of temperature change for all seasons over the whole basin area. In spring, the mean temperature is expected to increase between 2 °C and 4 °C by the end of the century. The highest increase can be expected over the southern part of the basin. In summer, temperature is expected to increase between 3 °C in the central part of the basin and 5 °C in the southern part of the basin. The temperature increase in summer is the most pronounced. In autumn, temperature is expected to increase between 2.5 °C in the central and 3.5 °C in the southern part of the basin. Strong warming can be observed also in winter, when temperature is expected to increase between 3 °C in the central and 4 °C in the southern part of the basin. In all seasons, the highest model spread for projections can be observed over complex orography (north-western part and western part of the basin). In general, temperature variability is expected to increase in all seasons towards the end of the century. The most significant increase in variability is expected for summer and winter. In spring and autumn, standard deviation is expected to increase by 1 °C by the end of the century, whereas in winter and summer the expected increase is approximately 1.5 °C for the whole basin.

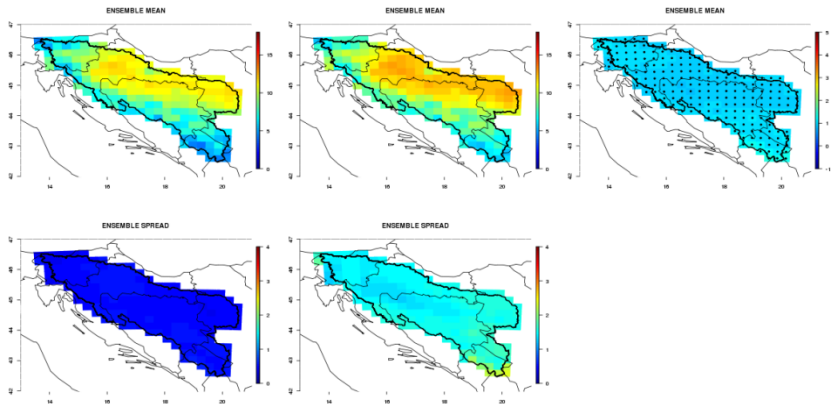

Figure 114: Projections of spring temperature. Shown are: ensemble mean and spread for the reference period (left column, unit is °C), ensemble mean and spread for 2011-2040 (middle column, unit is °C) and ensemble mean and spread of changes relative to the reference period (right column, unit is °C). Locations, where at least 80 % of models agree on the sign of change are marked with black dot.

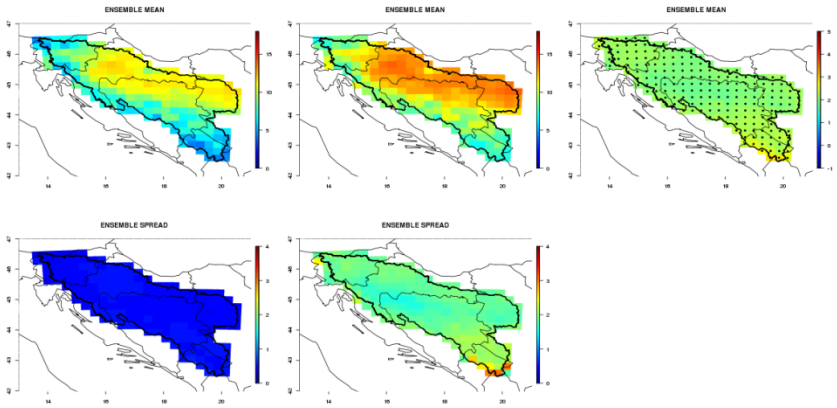

Figure 115: Projections of spring temperature. Shown are: ensemble mean and spread for the reference period (left column, unit is °C), ensemble mean and spread for 2041-2070 (middle column, unit is °C) and ensemble mean and spread of changes relative to the reference period

(right column, unit is °C). Locations, where at least 80 % of models agree on the sign of change are marked with black dot.

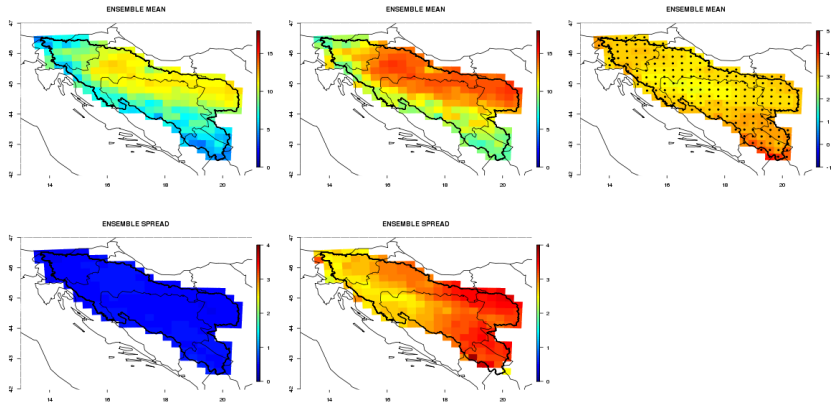

Figure 116: Projections of spring temperature. Shown are: ensemble mean and spread for the reference period (left column, unit is °C), ensemble mean and spread for 2071-2100 (middle column, unit is °C) and ensemble mean and spread of changes relative to the reference period (right column, unit is °C). Locations, where at least 80 % of models agree on the sign of change are marked with black dot.

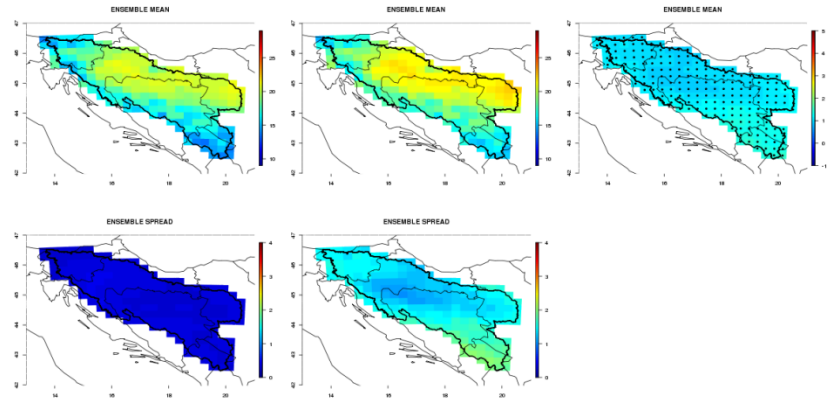

Figure 117: Projections of summer temperature. Shown are: ensemble mean and spread for the reference period (left column, unit is °C), ensemble mean and spread for 2011-2040 (middle column, unit is °C) and ensemble mean and spread of changes relative to the reference period (right column, unit is °C). Locations, where at least 80 % of models agree on the sign of change are marked with black dot.

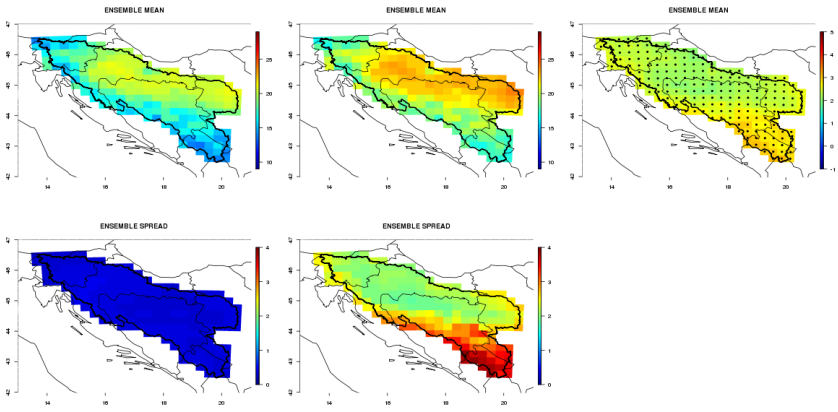

Figure 118: Projections of summer temperature. Shown are: ensemble mean and spread for the reference period (left column, unit is °C), ensemble mean and spread for 2041-2070 (middle

column, unit is °C) and ensemble mean and spread of changes relative to the reference period (right column, unit is °C). Locations, where at least 80 % of models agree on the sign of change are marked with black dot.

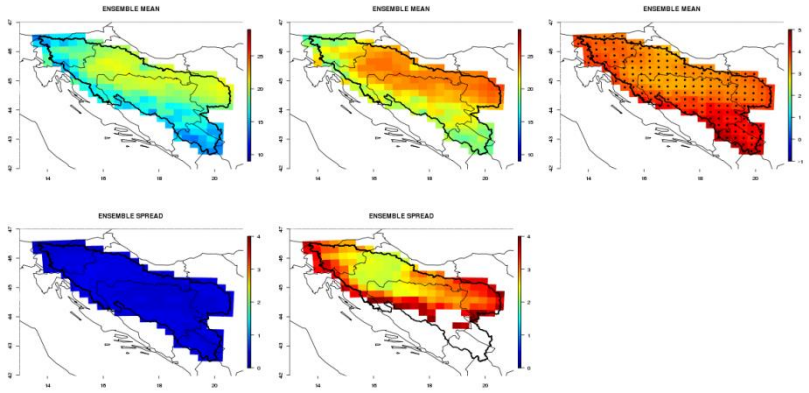

Figure 119: Projections of summer temperature. Shown are: ensemble mean and spread for the reference period (left column, unit is °C), ensemble mean and spread for 2071-2100 (middle column, unit is °C) and ensemble mean and spread of changes relative to the reference period (right column, unit is °C). Locations, where at least 80 % of models agree on the sign of change are marked with black dot.

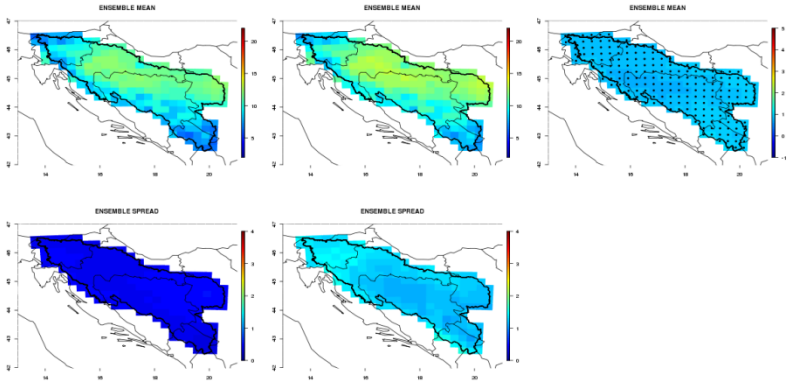

Figure 120: Projections of autumn temperature. Shown are: ensemble mean and spread for the reference period (left column, unit is °C), ensemble mean and spread for 2011-2040 (middle column, unit is °C) and ensemble mean and spread of changes relative to the reference period (right column, unit is °C). Locations, where at least 80 % of models agree on the sign of change are marked with black dot.

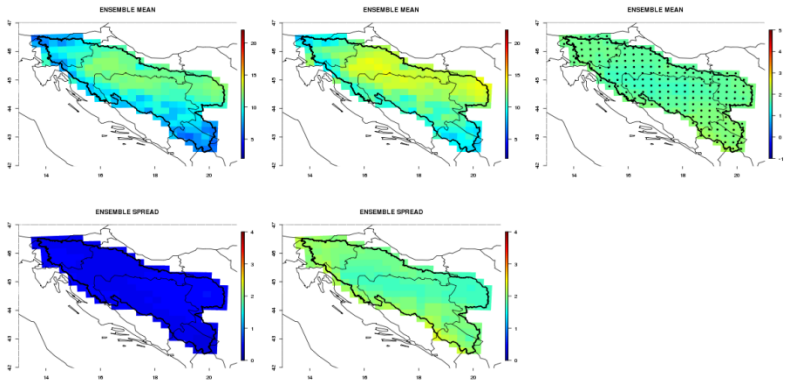

Figure 121: Projections of autumn temperature. Shown are: ensemble mean and spread for the reference period (left column, unit is °C), ensemble mean and spread for 2041-2070 (middle column, unit is °C) and ensemble mean and spread of changes relative to the reference period

(right column, unit is °C). Locations, where at least 80 % of models agree on the sign of change are marked with black dot.

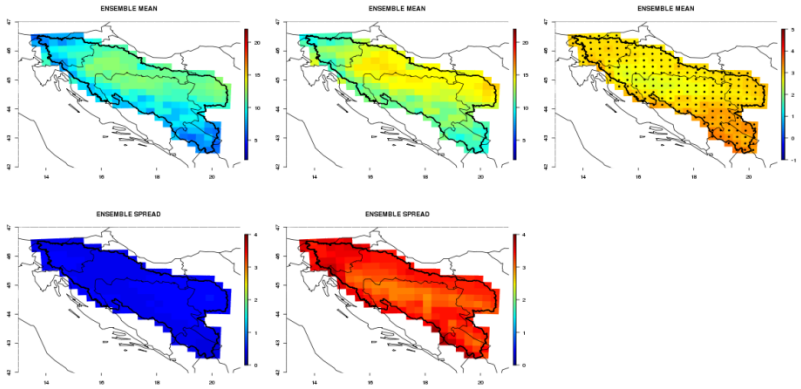

Figure 122: Projections of autumn temperature. Shown are: ensemble mean and spread for the reference period (left column, unit is °C), ensemble mean and spread for 2071-2100 (middle column, unit is °C) and ensemble mean and spread of changes relative to the reference period (right column, unit is °C). Locations, where at least 80 % of models agree on the sign of change are marked with black dot.

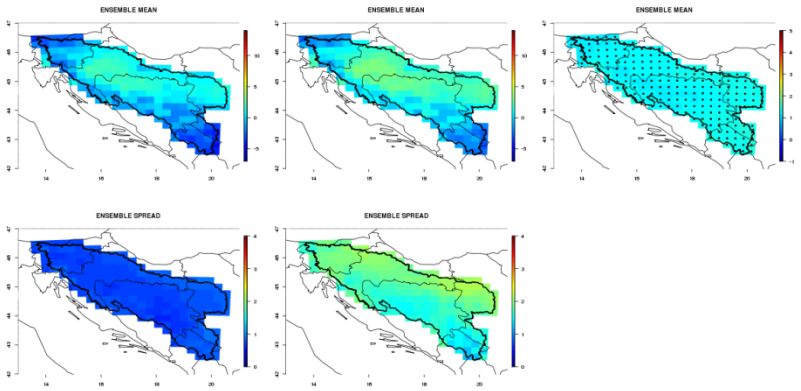

Figure 123: Projections of winter temperature. Shown are: ensemble mean and spread for the reference period (left column, unit is °C), ensemble mean and spread for 2011-2040 (middle column, unit is °C) and ensemble mean and spread of changes relative to the reference period (right column, unit is °C). Locations, where at least 80 % of models agree on the sign of change are marked with black dot.

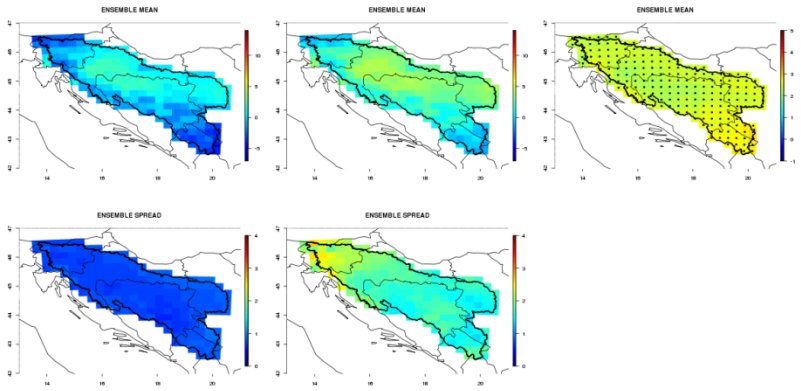

Figure 124: Projections of winter temperature. Shown are: ensemble mean and spread for the reference period (left column, unit is °C), ensemble mean and spread for 2041-2070 (middle column, unit is °C) and ensemble mean and spread of changes relative to the reference period (right column, unit is °C). Locations, where at least 80 % of models agree on the sign of change are marked with black dot.

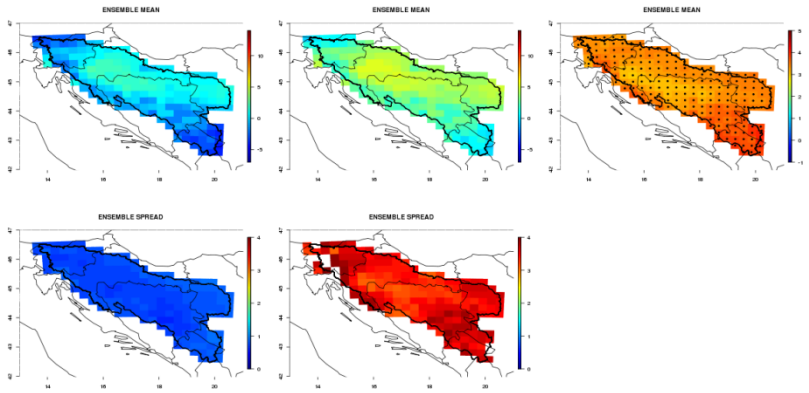

Figure 125: Projections of winter temperature. Shown are: ensemble mean and spread for the reference period (left column, unit is °C), ensemble mean and spread for 2071-2100 (middle column, unit is °C) and ensemble mean and spread of changes relative to the reference period (right column, unit is °C). Locations, where at least 80 % of models agree on the sign of change are marked with black dot.

5 CONCLUSIONS

ENSEMBLES climate model runs were used to produce climate projections for the Sava river basin. Statistical bias correction was used to correct raw model simulations for systematic biases. The validation procedure showed that the statistical bias correction improved the quality of daily precipitation and temperature simulations over majority of the basin area and was dependent on the season. Transfer functions, derived for the period 1961–2000, were used to produce climate change projections for the basin area. In general, temperature is expected to increase over the basin area in all seasons (the most pronounced increase can be observed for summer and winter). Precipitation is expected to decrease in spring, summer and autumn (with the most pronounced decrease in summer), whereas an increase in winter (especially in the north-western part of the basin) is expected.

In general, the highest model simulation spread was observed over the most complex orography (Julian Alps, Kamniško-Savinjske Alps and Dinaric Alps). This introduces some level of uncertainty in the simulation results over that area. In the future, climate model simulations of large-scale circulation patterns that influence the weather and climate in the basin should be verified. This will enable us to determine the primary causes of systematic model biases when simulating large-scale precipitation and other meteorological variables. A sensitivity study on convective parameterization schemes that are used in climate models to simulate sub-grid scale convective precipitation, would enable us to better understand and evaluate the uncertainty, related to extreme precipitation events over the basin area. In addition, the impact of changing model resolution should be analyzed in the future climate modeling experiments.

6 REFERENCES

Baigorria, G.A., Jones, J.W., Shin, D.W., Mishra, A. 2007. Assessing uncertainties in crop model simulations using daily bias-corrected Regional Circulation Model outputs. Climate Research, 34: 211–222

Boberg, F. et al., 2007, Analysis of temporal changes in precipitation intensities using PRUDENCE data. Danish Climate Centre Report, 07-03

Ceglar, A., Kajfež-Bogataj, L., 2012. Simulation of maize yield in current and changed climatic conditions: Addressing modeling uncertainties and the importance of bias correction in climate model simulations. European Journal of Agronomy. 37, 83–95

Christensen, J.H., Boberg, F., Christensen, O.B., Lucas-Picher, P. 2008. On the need for bias correction of regional climate change projections of temperature and precipitation. Geophysical Research Letters, p. L20709

Deque, M., Rowell, D.P., Luthi, D., Giorgi, F., Christensen, J.H., Rockel, B., Jacob, D., Kjellstrom, E., de Castro, M., van den Hurk, B., 2007. An intercomparison of regional climate simulations for Europe: assessing uncertainties in model projections. Climatic Change, 81, 53–70

Gilleland, Eric and Katz, Richard W. "Analyzing seasonal to interannual extreme weather and climate variability with the extremes toolkit (extRemes)", Preprints: 18th Conference on Climate Variability and Change, *86th American Meteorological Society (AMS) Annual Meeting*, **29** January - 2 February, 2006, Atlanta, Georgia. P2.15

Ines, A.V.M., Hansen, J.W. 2006. Bias correction of daily GCM rainfall for crop simulation studies. Agricultural and Forest Meteorology, 138: 44–53

Katz, R.W. 1999. Extreme value theory for precipitation: sensitivity analysis for climate change. Adv. Water Resour., 23, 133

Mearns, L.O., Bogardi, I., Giorgi, F., Matyasovszky, I., Palecki, M., 1999. Comparison of climate change scenarios generated from regional climate model experiments and statistical downscaling. J. Geophys. Res. 104, 6603–6621

Nakičenović, N., Alcamo, J., Davis, G., de Vries, B., Fenhann, J., Gaffin, S., Gregory, K., Grübler, A., Jung, T.Y., Kram, T., La Rovere, E.L., Michaelis, L., Mori, S., Morita, T., Pepper, W., Pitcher, H., Price, L., Riahi, K., Roehrl, A., Rogner, H.-H., Sankovski, A., Schlesinger, M., Shukla, P., Smith, S., Swart, R., van Rooijen, S., Victor, N., Dadi Z., 2000. IPCC Special Report on Emissions Scenarios. Cambridge University Press, Cambridge, United Kingdom and New York, NY, USA. 599 pp.

Perkins, S.E., Pitman, A.J., Holbrook, N.J., McAneney, J. 2007. Evaluation of the AR4 Climate Models Simulated Daily Maximum Temperature, Minimum Temperature, and Precipitation over Australia Using Probability Density Functions. Journal of Climate, 20: 4356–4376

Piani, C., Haerter, J.O., Coppola, E. 2010. Statistical bias correction for daily precipitation in regional climate models over Europe. Theoretical and Applied Climatology, 99: 187–192

Reaney, S.M., Fowler, H.J. 2008. Uncertainty estimation of climate change impacts on river flow incorporating stochastic downscaling and hydrological model parameterisation error sources. Durham, Durham University: 8 p.

Schneider, S.H. 2007. Contribution of working group 2 to the fourth assessment report of the intergovernmental panel on climate change. In: Climate Change 2007: impacts, adaptation and vulnerability. Parry, M.L, Canziani, O.F, Palutikof, J.P., van der Linden, P.J., Hanson, C.E. (eds.). Cambridge, Cambridge University Press: 779-810

Segui, P.Q., Ribes, A., Martin, E., Habets, F., Boe, J. 2009. Comparison of three downscaling methods in simulating the impact of climate change on the hydrology of Mediterranean basins. Journal of Hydrology, 383: 111–124

Semenov, M.A., Doblas-Reyes, F.J. 2007. Utility of dynamical seasonal forecasts in predicting crop yield. Climate Research, 60: 71–81

Sharma, D., Gupta, A.D., Babel, M.S. 2007. Spatial disaggregation of bias-corrected GCM precipitation for improved hydrologic simulation: Ping River Basin, Thailand. Hydrological Earth System Sciences, 11: 1373–1390

Tao, F., Yokozawa, M., Zhang, Z. 2009. Modelling the impacts of weather and climate variability on crop productivity over a large area: A new process-based model development, optimization, and uncertainties analysis. Agricultural and Forest Meteorology, 149, 5: 831–850

Trenberth, K.E., et al. 2003. The changing character of precipitation. Bulletin of American Meteorological Society, 84: 1205–1217

van der Linden, P., Mitchell, J.F.B. 2009. ENSEMBLES: Climate Change and its Impacts: Summary of research and results from the ENSEMBLES project. Exeter, Met. Office Hadley Centre: 160 pp.

Weigel, A.P., Liniger, M.A., Appenzeller, C. 2008. Can multi-model combination really enhance the prediction skill of probabilistic ensemble forecasts? Quarterly Journal of Royal Meteorological Society, 260: 241–260

Wood, A.W., Leung, L.R., Sridar, V., Lettenmaier, D.P., 2004. Hydrologic implications of dynamical and statistical approaches to downscaling climate model outputs. Climatic Change, 62, 189–216